Available online at www.sciencedirect.com
SCIENCE DIRECT®
Precambrian Research 132 (2004) 155–177
Precambrian Research
www.elsevier.com/locate/precamres

Source and tectono-metamorphic evolution of mafic and pelitic metasedimentary rocks from the central Quetico metasedimentary belt, Archean Superior Province of Canada

Franck Valli[a,*], Stephane Guillot[b], Kéiko H. Hattori[c]

[a] *Laboratoire de Tectonique, Mécanique de la Lithosphere, UMR7578 CNRS, Institut de Physique du Globe de Paris, 4 Place Jussieu, 75252 Paris cedex 05, France*
[b] *Laboratoire de Sciences de la Terre, UMR 5570 CNRS, UCB-Lyon et ENS-Lyon, 2 rue Dubois, 69622 Villeurbanne cedex, France*
[c] *Department of Earth Sciences, University of Ottawa, Ottawa, Ont., Canada K1N 6N5*

Received 11 December 2001; accepted 9 March 2004

Abstract

A study of the sedimentary rocks in the Jean Lake area of the Quetico metasedimentary belt, Superior Province, Canada, was conducted in order to evaluate the origin, source, and evolution of rocks, including mafic rocks previously mapped as ultramafics rocks. Bulk compositions of these sedimentary rocks show a mixing between two end members: quartzo-feldspathic sedimentary rock and komatiitic basalt. High CaO and MgO contents of the rocks suggest a proximal source of the komatiitic basalt.

The rocks in the study area record a pressure–temperature (*P*–*T*) path with three tectono-metamorphic stages. The first stage formed staurolite (500–700 °C) under medium *P*–*T* (MP–MT) metamorphic conditions shortly after the sedimentation. The second stage yielded the biotite–sillimanite–garnet assemblage under the peak conditions of 0.6 ± 0.1 GPa and 700 ± 70 °C during transpressional deformation. The third stage, low *P*–medium *T* (LP–MT; 0.25 ± 0.11 GPa, 540 ± 80 °C) metamorphism, was associated with regional south-southeast compression and its timing is constrained by a new U–Th–Pb monazite age of 2667 ± 20 Ma. Combining the regional deformation events, we suggest the burial metamorphism of sediments up to MP–MT conditions during the D1 deformation at 2698–2689 Ma. They attained the peak metamorphic conditions during the regional transpressive D2–D3 deformation (2689–2671 Ma), and retrograded to LP–MT condition during the south-southeast compression (regional D4) at 2671–2667 Ma.

A short time span between the sedimentation and MP–MT metamorphism accompanied by D1 deformation suggest that the Quetico sedimentary rocks formed in an acretionary prism. The studied rocks in the Jean Lake area deposited close to the Wabigoon Subprovince, transported towards the south, and buried up to ∼20 km by rapid underthrusting to amphibolite facies conditions. Subsequent dextral transpressive deformation (D2–D3) during the oblique docking of the Quetico belt to the Wabigoon Subprovince to the north and Wawa greenstone belt from the south resulted in the displacement of the sedimentary rocks to the west from the original depositional site. The *P*–*T*–time path of the Quetico sedimentary rocks is similar to that in modern arc accretion prisms, except for a high geothermal gradient of ∼30 °C/km recorded in the former compared to ∼10 °C/km

* Corresponding author. Tel.: +33-1-4427-2439; fax: +33-1-4427-2440.
E-mail address: valli@ipgp.jussieu.fr (F. Valli).

0301-9268/$ – see front matter
doi:10.1016/j.precamres.2004.03.002

in modern counterparts. The high temperature gradient in the Archean accretionary prism explains the lack of high-pressure metamorphic rocks, such as blueschist, that are common in modern accretionary prisms.

Keywords: Archean tectonics; Archean accretionary prism; Provenance; Geochemistry of clastic sedimentary rocks; Geothermal gradient; Archean subduction zone; Monazite geochronology

1. Introduction

The Archean Superior Province contains linear arrays of granite-greenstone belts and metasedimentary belts. Successive accretion of volcanic arcs in late Archean time (Card, 1990; Thurston and Chivers, 1990; Fig. 1) is considered as a likely process for the formation of the Archean craton. This is supported by "frozen subduction zones" shown in seismic reflection profiles across the Canadian Shield (Ludden et al., 1993; Calvert et al., 1995; Cook et al., 1999). Metasedimentary belts between greenstone belts may represent accretionary prisms developed during subduction and collision of arcs (Percival, 1989; Card, 1990; Williams, 1990).

The Quetico Subprovince is one such metasedimentary belt in the western Superior Province and is bounded by two volcanic belts: the Wabigoon Subprovince to the north and by the Wawa Subprovince to the south (Figs. 1 and 2). The Quetico Subprovince consists mostly of turbiditic Qtz-rich metasedimentary rocks with minor banded iron formations. In this monotonous sedimentary belt, a lens of "ultramafic rocks", ∼2 km long and 400 m wide, crops out around Jean Lake, north of Lake Superior (Williams, 1988, 1991; Fralick et al., 1992; Fig. 2). Earlier

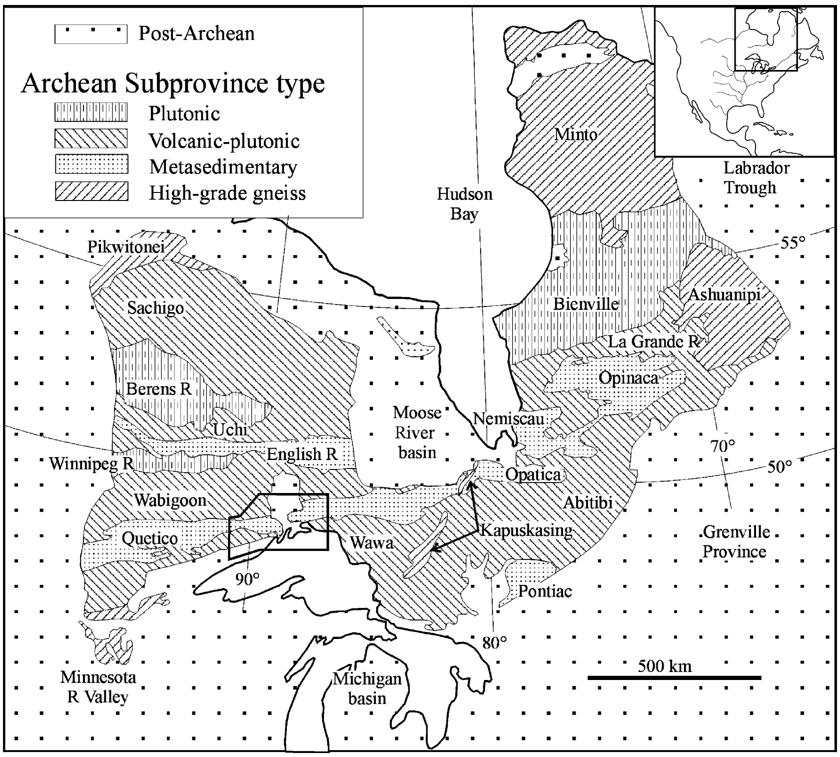

Fig. 1. Simplified geological map of the Superior Province with the location of the study area shown in Fig. 2, modified after Card (1990).

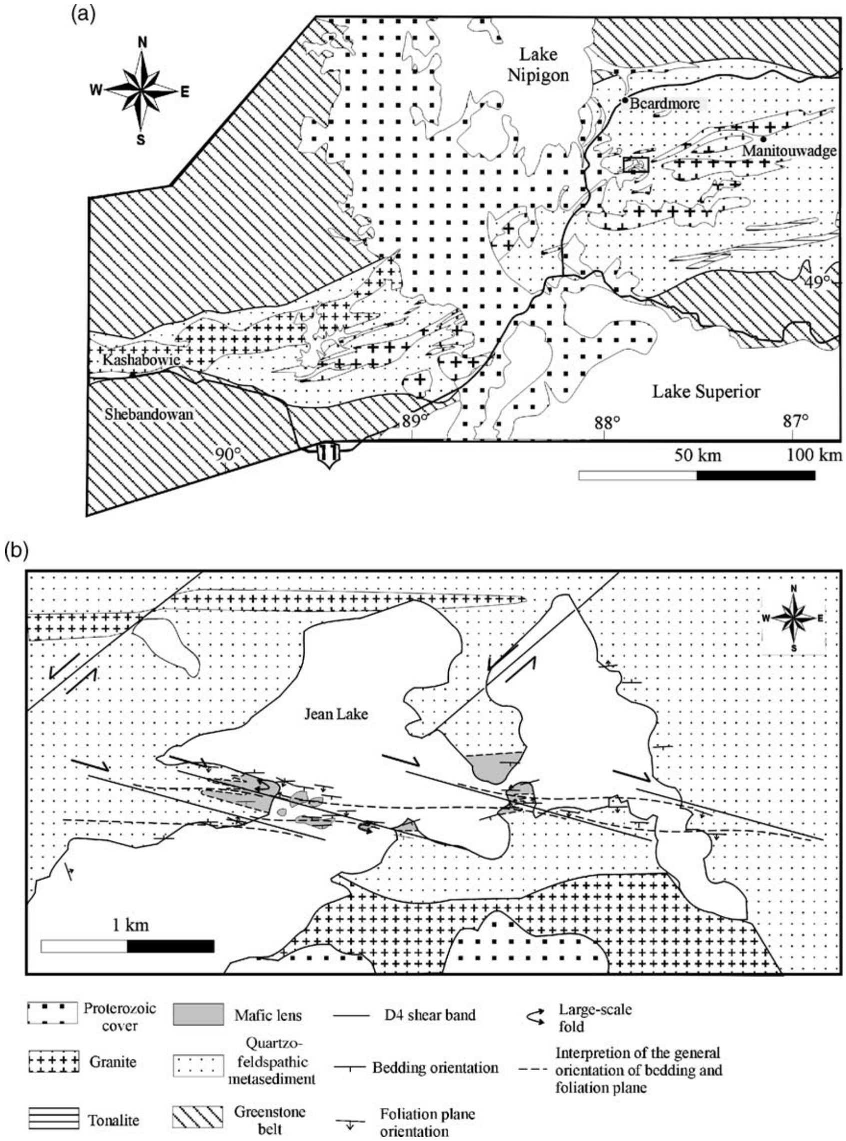

Fig. 2. (a) Geological map of the central Quetico metasedimentary belt (modified after map 2542 from Ontario Geological Survey, 1991) and the location of the study area. (b) Geological map of the study area (modified after map 2056 by Pye, 1964). Structural measurements and geological contours of the mafic lens are from this study.

work suggested that this lens formed by weathering of ophiolites or serpentinite diapirs (Williams, 1988, 1990; Fralick et al., 1992). Ophiolites and serpentinite diapirs are common in modern convergent margins (Nicolas, 1989; Fryer et al., 1995), but their occurrence of Archean age is in debate (e.g. Hamilton, 1998; De Wit, 1998). Therefore, the "ultramafic" unit in the Quetico belt may provide information relevant to Archean tectonics, and may shed additional light on the evolution of the Quetico metasedimentary belt. In addition, the deformation of the Quetico sedimentary rocks are poorly dated and the prograde path of their metamorphic evolution has not been studied. Such information will contribute to better understanding of the origin of the belt. Consequently, a study of the “ultramafic” rocks was conducted with four objectives: (i) to characterize the “ultramafic” rocks, (ii) to evaluate their origin and source, (iii) to examine the structural and metamorphic evolution of the “ultramafic” and surrounding rocks, and (iv) to compare the Quetico belt with modern accretionary prisms.

2. Geological setting

The Quetico Subprovince is a linear belt of dominantly Qtz-rich, turbiditic metagraywackes (Ojakangas, 1985) that has a relatively consistent width of about 70 km and extends approximately 1200 km from longitude 70–96 °W (Williams, 1991). The timing of sedimentation is constrained, by the youngest U–Pb age of zircon in the sedimentary rocks and the oldest age of intrusions. These ages are significantly different between the northern and southern parts of the belt. The youngest age of zircon in the northern part is 2698 ± 3 Ma, whereas that in the southern part is 2688.5 ± 1 Ma (Zaleski et al., 1999; Davis et al., 1990). The oldest U–Pb zircon intrusion age is 2696 ± 2 Ma in the northern Quetico belt and 2670.5 ± 2 Ma for granitic intrusions in the south Quetico belt (Percival and Sullivan, 1988; Percival, 1989; Williams, 1991). The data suggest that the southern part deposited significantly later than the northern part.

Igneous rocks are minor in the Quetico belt. They include rare felsic volcanic rocks (Williams, 1991), tonalitic–granodioritic intrusions dated at 2696 Ma (Davis et al., 1990; Zaleski et al., 1999), a suite of carbonate-bearing alkaline complexes of 2680 ± 1 Ma (Hattori and Percival, 1999; Lassen et al., 2000), and large aluminous granites dated between ∼2670 and ∼2650 Ma (Percival, 1989; Williams, 1991).

The Wabigoon Subprovince to the north consists of igneous rocks formed during several magmatic pulses: 3005–2990 Ma mafic–felsic volcanic and tonalite complexes, 2750–2700 Ma mafic–felsic volcanic rocks and ∼2690 Ma monzodiorite–diorite and mafic–ultramafic suites (Sutcliffe et al., 1989; Blackburn et al., 1991). The Wawa Subprovince, to the south, is composed of 2750–2690 Ma old ultramafic, mafic, and felsic volcanic rocks and related intrusions (Williams, 1990).

3. Occurrence of mafic rocks in the Jean Lake area

3.1. Distribution and lithology

The “ultramafic” lens is well exposed on the shores and on small islands in the Jean Lake (Fig. 2). Rocks contain millimeter-size clasts of quartz aggregates and exhibit sedimentary textures, including climbing ripples, flame structure, loading, and stratification (Fig. 3a–c). These observations suggest a sedimentary origin of these rocks. Bedding and foliation strike east, dip mainly south (between 85° north and 50° south) and the “ultramafic” lens is surrounded by quartzo-feldspathic metasedimentary rocks similar to those in the remainder of the Quetico belt.

The quartzo-feldspathic rocks consist of two lithological units, a volumetrically dominant semi-aluminous unit (45–25 vol.% of Qtz, 50–30 vol.% of Pl, 35–10 vol.% of Bt, <35 vol.% of Chl, <10 vol.% of Ms, and <10 vol.% of Grt, abbreviations are from Kretz, 1983) and a minor aluminous unit (40–25 vol.% of Qtz, 40–30 vol.% of Pl, 30–20 vol.% of Bt, 30–5 vol.% of St, <10 vol.% of Chl, <5 vol.% of Ms, and <5% of Grt). The “ultramafic lens” contains three units; Bt–amphibole-rich unit, amphibole-rich unit, and felsic unit. All units contain more than 10 vol.% of felsic minerals (Qtz and feldspars), and are thus, mafic rather than ultramafic. The biotite–amphibole-rich unit is made of 40–10 vol.% of Qtz, 35–10 vol.% of Pl, 50–5 vol.% of amphibole, 40–5 vol.% of Bt, and <40 vol.% of Chl. The amphibole-rich unit contains 90–40 vol.% of amphibole, 20–5% of Qtz, 20–5% of Pl, and <10 vol.% of Chl.

The felsic unit is identical to the surrounding quartzo-feldspathic rocks. Unit names instead of rock names are used in this manuscript because the unit names can best characterize the studied rocks which are highly heterogeneous in mineral abundance.

The decameter to meter lenses of amphibole-rich rock unit occurs parallel to the bedding and form high relief on the weathered surface of the hosting, biotite–amphibole-rich unit. South and north of the Jean Lake, sedimentary rocks are cut by granitic dykes and sills, which originated from the voluminous, two mica granite of 2670–2650 Ma (Percival, 1989; Williams, 1991).

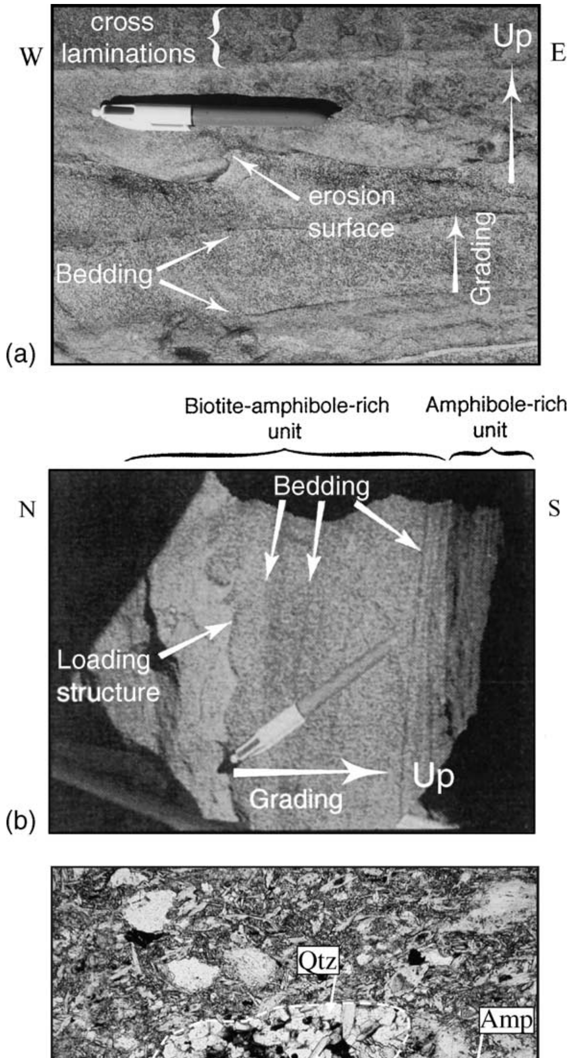

Fig. 3. (a) Sedimentary structures of the quartzo-feldspathic turbiditic rock. Pen is 14 cm long. Bedding in the middle section under the erosion surface, cross lamination in the top portion of the photograph. and grain size sorting in the bottom part of the outcrop. (b) Loading structure, bedding, and sedimentary grading in the biotite–amphibole-rich unit and amphibole-rich unit. (c) Photomicrograph showing a quartz-rich clast in the amphibole-rich unit. This section was made in the amphibole-rich unit of the sample shown in (b).

3.2. Chemical composition and source of the mafic sedimentary rocks

The mafic sedimentary rocks show significant compositional variations (Table 1). The contents of SiO_2, Al_2O_3, MgO, and Cr vary from 53.9 to 65.5 wt.%; 9.8 to 17.9, 3.0 to 12.5 wt.%, and 149 to 866 ppm, respectively (Table 1). The contents of Al, Ti, Mg, and Cr form linear arrays with high correlation coefficients ($r > 0.95$), suggesting that they were immobile after sedimentation (Rollinson, 1993). Linear arrays of Ca, Ga, V, Zn, Co, and Ni against these immobile elements suggest that they too were relatively immobile. The plot of two immobile elements, such as TiO_2 versus Al_2O_3, shows a linear array between the felsic and amphibole-rich units and the biotite–amphibole-rich unit plot between the two units (Fig. 4).

There are three possible causes to form the linear arrays; constant sum effect, hydraulic sorting, and mixing of two end-members. The constant sum effect is rejected because elemental ratios, such as Ti/Mg and Al/Mg, also show linear arrays (Fig. 5a). Hydraulic sorting from a single source was suggested for the cause of compositional variation of sedimentary rocks from the area between the Beardmore and Jean Lake area (Fralick and Kronberg, 1997). The high Cr contents (up to 866 ppm) imply contribution of chromite to the sedimentary rocks. Moreover, the positive correlation between Cr and Ca contents requires contributions of Ca-minerals and chromite with similar proportion to the sediments; an unlikely condition because these two minerals have very different densities.

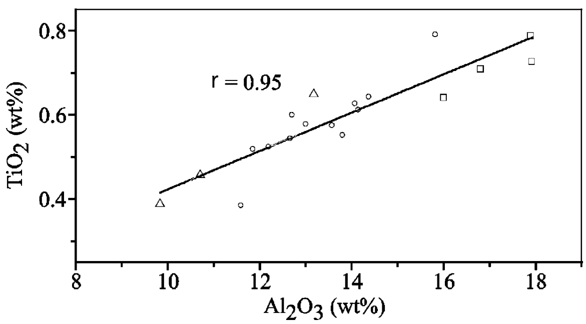

Fig. 4. TiO_2 vs. Al_2O_3 wt.% of mafic rocks in the Jean Lake area. Circles correspond to the rocks from the biotite–amphibole-rich unit; triangle: rocks from the amphibole-rich unit; square: felsic unit in the mafic lens and quartzo-feldspathic rocks surrounding the mafic lens.

Table 1
Bulk chemical composition of representative rocks from the Jean Lake area

	Amphibole-rich unit $^{\Omega}$					Biotite–amphibole-rich unit $^{\Omega}$							Felsic-unit and host rocks $^{\Omega}$							Kom. basalt $^{\Omega}$	Harz $^{\Omega}$	Lherz $^{\Omega}$
	227b	239d	239a	252a	227c	230	237	239c	239e	243	246b	252b	265c	268d	265a	236	239b	246a	249			
SiO_2	58.20	59.19	54.43	63.14	57.10	56.41	59.75	56.75	55.25	56.52	63.19	60.92	53.90	57.02	60.66	56.29	65.51	59.26	58.99	47.60	39.77	44.56
TiO_2	0.46	0.39	0.65	0.58	0.52	0.61	0.60	0.54	0.63	0.79	0.64	0.64	0.53	0.58	0.39	0.79	0.55	0.73	0.71	0.46	0.01	0.06
Al_2O_3	10.70	9.82	13.17	13.0	11.84	14.13	12.69	12.65	14.06	15.81	15.99	14.36	12.18	13.56	11.58	17.88	13.79	17.91	16.79	10.60	0.38	2.42
Fe_2O_3 *	6.65	6.33	9.21	7.23	6.56	8.06	7.89	7.39	7.18	7.02	6.71	7.95	7.50	6.66	4.78	9.46	5.95	8.38	7.77	11.36	9.18	8.43
MnO	0.14	0.16	0.16	0.16	0.11	0.12	0.13	0.12	0.09	0.10	0.15	0.13	0.12	0.11	0.12	0.11	0.08	0.09	0.09	0.19	0.08	0.12
MgO	10.49	10.45	9.43	4.39	11.20	7.37	7.14	10.36	10.66	6.14	2.96	4.87	12.49	9.45	8.43	4.23	3.77	3.68	3.29	13.8	36.83	40.47
CaO	7.52	8.86	5.89	6.80	4.76	5.62	5.15	4.21	2.81	4.55	2.83	3.88	5.85	4.35	8.38	1.68	2.52	1.67	2.08	11.9	0.26	2.20
Na_2O	1.93	2.08	1.9	3.08	2.04	2.48	2.39	1.79	2.04	3.45	1.03	3.07	1.49	2.14	1.99	2.21	3.36	2.07	2.88	0.83	0.17	0.03
K_2O	0.97	0.31	2.75	0.24	1.59	2.74	2.11	2.66	2.39	2.98	3.47	2.21	2.33	2.99	0.90	4.16	2.20	3.22	3.85	0	0.01	
P_2O_5	0.19	0.17	0.16	0.09	0.23	0.25	0.15	0.18	0.24	0.37	0.13	0.15	0.21	0.19	0.38	0.14	0.12	0.15	0.17	0.03	0.05	0.06
LOI **	1.8	1.3	1.9	0.5	4.7	1.3	2.6	2.2	3.4	1.2	1.8	1.2	2.80	1.9	1.4	2	2.1	1.9	1.4	1.8	13	1.27
V	115	109	157	151	104	125	140	107	111	127	136	140	117	115	104	195	105	162	143			61
Cr	685	808	866	417	349	570	586	670	406	436	149	370	716	407	451	192	191	170	165	994	3362	2770
Co	36	44	42	30	34	34	34	40	40	28	22	26	43	29	20	27	13	30	28	56	102	
Ni	410	503	229	127	327	169	172	394	425	132	80	94	437	214	190	73	49	89	97	300	2358	2330
Zn	54	57	95	72	67	86	82	81	73	77	79	80	73	69	39	88	71	88	97	69	72	
Rb	31	9	99	5	51	86	71	84	80	105	150	82	74	97	46	134	71	108	158			
Sr	528	281	278	295	522	614	292	275	285	392	202	352	330	284	469	225	388	205	326	68		1.1
Y	14	14	16	16	20	14	14	14	13	16	16	16	15	16	18	16	13	18	17	10		2.3
Zr	112	83	125	134	129	140	117	126	132	178	127	130	122	137	89	118	133	120	145	36	1.2	0.4
Nb	10	9	7	7	6	8	6	7	12	10	8	7	9	8	10	9	7	9	9			
Ba	281	138	843	40	387	771	766	870	688	865	604	603	622	756	113	918	488	584	955	50	0	
La	<10	<10	31	33	39	25	<10	37	21	36	15	28	22	26	13	26	25	36	40	2.08	0	
Ce	36	33	34	67	78	56	17	37	55	83	52	27	23	31	33	41	24	65	91	4.21	0	
Nd	<10	18	<10	20	18	27	<10	21	23	47	19	<10	12	14	23	<10	13	14	34	3.45	0	
Pb	8	12	<1	<1	<0.0	<1	4	2	<1	5	<1	3	<1	<1	4	1	6	1	20		21	
Th	6.85	3.92	6.31	6.92	6.43	5.57	5.88	6.97	9.21	9.32	8.28	8.11	7.54	9.14	3.19	7.59	5.79	7.55	9.63			
Ga	10.4	10.8	17.3	14.5	14	15.8	16.3	15.6	16.2	19.2	19.1	17.2	14.6	16.8	11.2	23.2	15.2	21.2	20.2			2
Total	99.28	99.26	99.93	99.33	100.8	99.36	100.8	99.14	98.98	99.2	99.08	99.58	99.66	99.15	99.18	99.15	100.1	99.24	98.26	98.57	99.74	99.97

Uranium contents were all below detection limit of 1 ppm. Kom. basalt: komatiitic basalt from Wabigoon (Ayer, 1999). Harz: harzburgite from the Mariana fore arc (Yamamoto et al., 1992). Lherz: lherzolitic composition (Ballantyne, 1992).

$^{\Omega}$ Oxides are in wt.% and other elements in ppm.

* Total Fe expressed as Fe_2O_3.

** Loss of ignition.

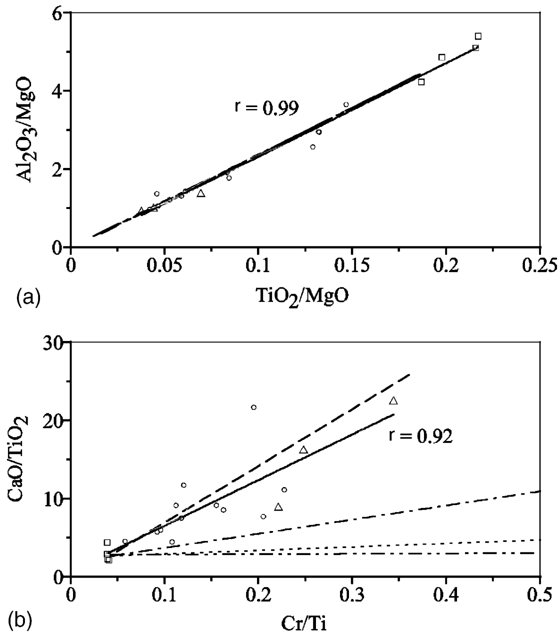

Fig. 5. (a) Weight ratios of Al_2O_3/MgO vs. TiO_2/MgO for rocks from the mafic lens in the Jean Lake area. The regression line (solid line) of sedimentary rocks from the mafic lens compared to various mixing lines between an average composition of the Quetico quartzo fedspatic sedimentary rocks (host rocks and felsic-unit rocks) and possible ultramafic and mafic rocks; komatiitic basalt (dashed line; Ayer, 1999), komatiite (dash-dot line; Ayer, 1999) in the southern Wabigoon Subprovince, harzburgite (dash-double-dot line; Yamamoto et al., 1992) and lherzolite (dotted line; Ballantyne, 1992). (b) Weight ratios of CaO/TiO_2 vs. Cr/Ti for rocks from the mafic lens in the Jean Lake area. Line types same as in (a).

Linear correlations of elements are thus attributed to the mixing of end-member components.

The amphibole-rich unit contains high MgO (up to 12.5 wt.%), Cr (up to 866 ppm), and high PGE (20 ppb Pt, 17 ppb Pd, 3 ppb Ir). These values are all greater than those of most basaltic igneous rocks, suggesting a contribution from more Mg-rich rocks such as komatiitic basalts, komatiites, and mantle peridotites. The latter two possibilities are rejected because of too low CaO contents of komatiites and mantle peridotites to account for our samples (Fig. 5b). This leaves komatiitic basalts as the source. The amount of the komatiitic basalts is calculated to be nil in the felsic unit and up to ~90% in the amphibole-rich unit using the lever rule (Fig. 5b).

4. Deformation in the Jean Lake area and correlation with regional deformation

Four tectono-metamorphic events have been recognized in the Quetico Subprovince (Williams, 1991, and references therein). The first regional deformation (D1) included slumping, and recumbent folding shortly after sedimentation (2698 to <2690 Ma; Table 4; Sawyer, 1983; Williams, 1991; Zaleski et al., 1999). This event was followed by mainly dextral strike-slip shearing (D2) which resulted in the formation of a Subprovince scale west-trending vertical planar fabric, and lineations plunging east at 10–30° (Williams, 1991). The subsequent deformation was also transpressive (D3), and produced upright folds (F3) that affected both the bedding and the earlier-formed planar fabrics (Sawyer, 1983; Williams, 1991). The D4 deformation corresponds to minor shearing under a south-southeast compression (Sawyer, 1983).

The study area shows only three stages of deformation. The first stage of deformation in the Jean Lake area produced a foliation defined by Bt and St. The foliation was later folded during the main deformation event in the area, producing decimeter-scale tight folds with an axial trace of N95 80S. The later foliation, which is defined by Bt, Grt, and Sil, is locally oblique to this main axial surface direction in hinges of larger-scale upright folds (Fig. 2). Similar upright folds are common in the Quetico belt and considered to have formed under the regional transpressive D3 deformation (part 4; Williams, 1991), suggesting that this later foliation and upright folds in the Jean Lake area are most like a product of the regional D3 deformation. It implies that the earlier foliation in the Jean Lake area formed during either D1 or D2 regional deformation.

The final deformation in the Jean Lake area produced local shear zones, which are defined by Chl ± Bt ± amphibole, strike N110°, dip steeply to the south (Fig. 2). They cut earlier planar and folded fabrics (pre-S3 and S3) and bedding planes and east-trending pre-S3 and S3 foliations rotate into the shear planes, forming hectometer-scale dextral sigmoïds. Z-folds, which also suggest the presence of dextral strike-slip motion are located on both flanks of F3 folds suggesting that they are not drag folds, but folds posterior to F3 (F4). Narrow (up to 1 cm width) Qtz veins show Z-folds inside the shear zones and the folding likely developed during this dextral shearing (Fig. 6a). The geometry of centimeter-wide kink bands of Chl is also consistent with dextral shearing along a N110° direction. Pye (1964) identified N50° sinistral shear planes in the Jean Lake area (Fig. 2) and these planes may be a conjugate with the observed N110° dextral shear plane under south-southeast compression. Sawyer (1983) documented similar conjugate ductile shears and semi-brittle deformation features which were formed under a south-southeast compression in the Kashabowie area (∼200 km south-east of the Jean Lake area). This defines the regional D4 deformation.

5. Metamorphism in the Jean Lake area

5.1. Mineralogy and mineral chemistry

We conducted a detailed thermobarometric study of the felsic and amphibole-rich units, which represent the end members of the compositional variations in the study area.

5.1.1. Aluminous unit

The rocks are defined by the following minerals: Qtz + Pl + Bt + St ± Grt ± Sil ± Chl ± Ilm ± Tur. Both Qtz and Pl, ranging from 0.05 to 0.1 mm in size, are anhedral in shape and Pl is homogenous in composition (An25–27). Bt (up to 2 mm in length) defines the pre-S3 foliation, subsequently deformed by F3 folds. Later Bt, Bt_2, crystallized parallel to the axial surface, forming the S3 foliation. Bt_2 in contact with Grt, St, and in the matrix have similar compositions with X_{Fe} (=Fe/(Fe + Mg) atomic ratio) of 0.47–0.49 (Table 2). St (up to 0.5 cm; 30–5 vol.%, X_{Fe} from 0.82 to 0.84) is anhedral with corroded rims and belongs to the pre-S3 foliation. Folded crystals, outline the noses of some centimeter-scale tight F3 folds (Fig. 6c).

Rare fibrous Sil occurs parallel to the S3 foliation between corroded St and euhedral Bt and Grt (Fig. 6d). The texture suggests the following KFMASH reaction:

$$\mathrm{St + Qtz + Bt_1 = Bt_2 + Sil + Grt + H_2O} \qquad (1)$$

Grt porphyroblasts (0.2–1.0 mm) are euhedral and contain Qtz inclusions, and crystallized during the development of the main S3 foliation. They are solid solutions of $Alm_{0.72–0.78}$, $Prp_{0.10–0.14}$, $Grs_{0.03–0.07}$, and $Sps_{0.07–0.08}$, and show increasing Alm component toward the rims (Fig. 7). The Sps component decreases towards rims and increases within the 70 μm thick rims (Fig. 7). The bell shaped profile of Ca and Mn with a gentle increase in X_{Fe} towards the rims is commonly formed during crystal growth (Spear, 1993; Reaction 1). The sharp increase of Fe in the outermost rims is probably related to late diffusion of Fe from Bt_2, as suggested by Spear (1993).

Bt grains are homogeneous, probably because of fast elemental diffusion in Bt (Spear, 1993). They are partially replaced by Chl.

5.1.2. Semi-aluminous unit

This unit consists of Qtz + Pl + Bt ± Grt ± Chl ± Ilm ± Tur. Anhedral Qtz (0.05–0.1 mm) is predominant and Pl crystals (0.05–0.2 mm) are anhedral and commonly contain Qtz inclusions. Individual grains do not show compositional zoning, with $An_{0.24–0.31}$ and $An_{0.14}$ in sample 244 and $An_{0.22–0.27}$ in sample 262b (Table 2).

Bt (0.1–0.3 mm) defines the main S3 foliation and re-crystallized in D4 shear bands (Fig. 6b). Some Bt surrounding Grt define delta micro-structures. Bt grains in contact with Grt have similar compositions as those in the matrix, with X_{Fe} of 0.48–0.49.

Euhedral Grt grains (0.3–1.2 mm) contain rounded Qtz inclusions and were rotated by the late dextral strike-slip shear deformation (D4), suggesting crystallization before or during D4. In sample 262b, Grt crystals (∼1 mm) have Alm component ranging from 0.78 to 0.84, whereas Grt (∼0.7 mm) in sample 244 contains between 0.67 and 0.73 Alm component (Table 2). Sps, Grs, and Prp components vary from 0.17 to 0.13, 0.06 to 0.04, and 0.12 to 0.10, respectively. The Grs and Sps components and X_{Fe} decrease from core to rim. The 80 μm-thick rims record a reverse trend; an increase in Sps and X_{Fe}, and a decrease in Prp component (Fig. 7).

This bell-shaped zoning pattern suggests that the zoning is a result of crystal growth without subsequent modification by diffusion (Fig. 7). The reverse zoning in the outer rim implies a consumption of Grt during retrogression (Spear, 1993).

Anhedral Kfs crystals identified in one sample occur around Grt porphyroblasts in association with Chl suggest the following reaction:

$$\mathrm{Grt + Bt + H_2O = Kfs + Chl} \qquad (2)$$

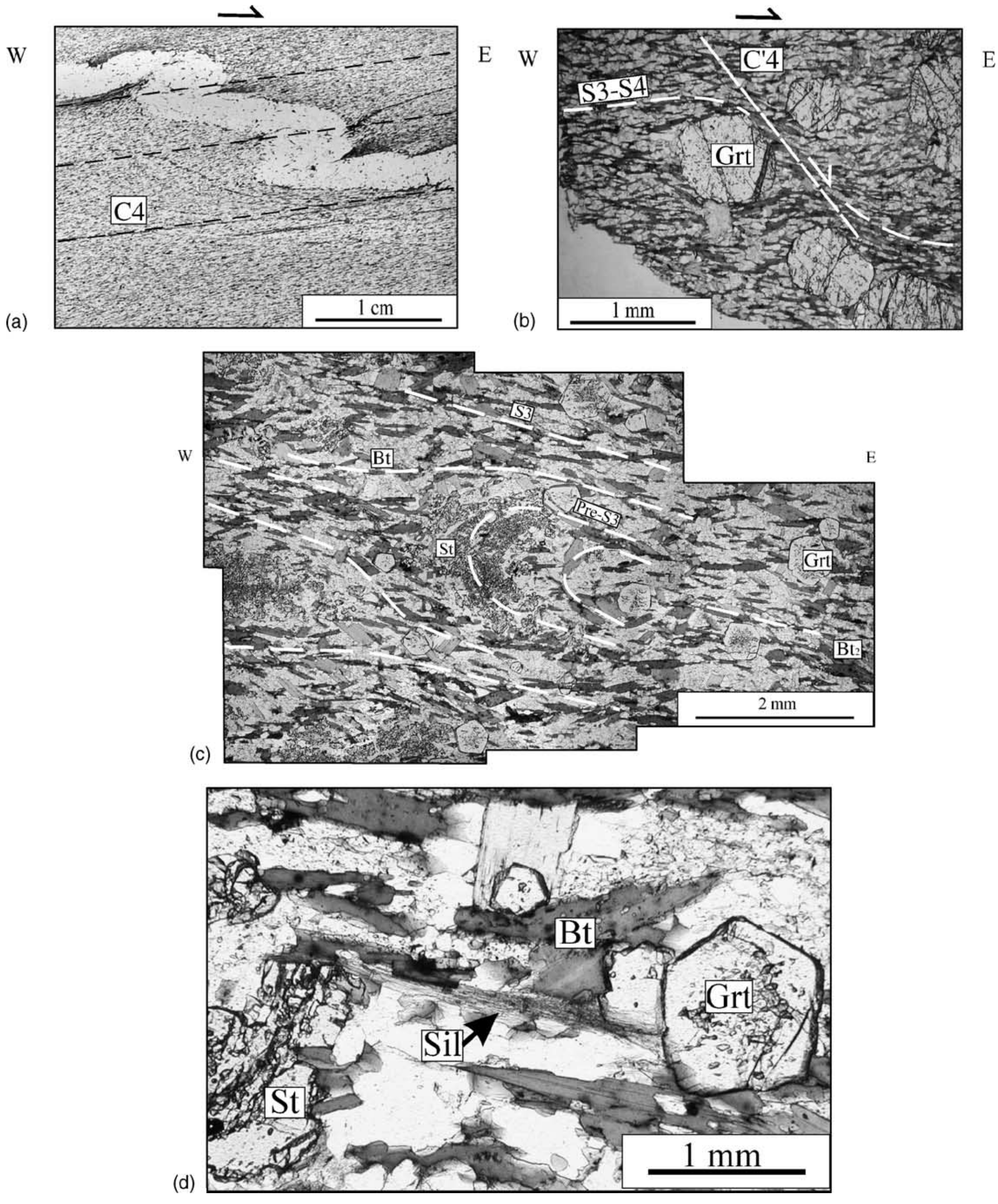

Fig. 6. (a) Photomicrograph showing a Z-folded quartz vein parallel to D4 shear planes in the semi-aluminous unit (sample 219). Thin section perpendicular to the shear plane. (b) Photomicrograph of a sample of the semi-aluminous unit (sample 262b). S2–S3 foliation defined by biotite is transposed into dextral C4 shear bands, and cut by C′4 shear planes. Thin section perpendicular to the foliation plane. (c) Photomicrograph of a sample of the aluminous unit (sample 251). Staurolite (St) and earlier formed biotite (Bt) are folded by D3 event. A new foliation (S2–S3) defined by biotite (Bt_2) develops parallel to the axial plane. Note the folded grain of St at the nose of the tight fold. (d) Photomicrograph of a sample of quartzo-feldspathic unit (sample 251). Staurolite is replaced by garnet (Grt), biotite (Bt), and sillimanite (Sil).

Table 2
Representative mineral compositions used for the *P*–*T* estimate for the peak and LP–HT metamorphic events

Samples[α]	Garnet				Biotite					Plagioclase						St	Amphibole	
	251 Rev[γ]	262b Rev[γ]	244 Rev[γ]	244 Rim	251	251 Rim	262b	244		251	262b	244	244 Ret[χ]	268a	252a	251	268a	252a
SiO_2	36.82	36.81	36.87	37.58	35.74	35.70	35.38	35.92		62.45	61.25	63.92	59.73	59.08	59.86	27.62	48.97	43.52
TiO_2	0.05	0.05	0.01	0.02	1.76	1.89	1.52	1.61		0.00	0.00	0.00	0.04	0.04	0.00	0.54	0.30	0.68
Al_2O_3	21.31	20.66	21.35	21.35	19.23	19.20	18.36	18.00		23.77	23.99	21.93	24.61	26.17	25.56	55.75	9.49	12.47
[β]FeO	34.72	37.37	32.04	32.48	17.90	17.86	20.93	18.95		0.25	0.25	0.44	0.33	0.27	0.30	13.86	9.52	16.41
MnO	3.05	0.33	5.98	5.80	0.08	0.09	0.00	0.09		0.00	0.00	0.00	0.0	0.00	0.00	0.04	0.23	0.35
MgO	3.43	3.11	2.87	2.69	10.63	10.28	9.50	10.84		0.00	0.00	0.00	0.00	0.01	0.00	1.55	14.77	9.78
CaO	1.70	1.60	1.45	1.26	0.02	0.01	0.00	0.08		5.08	5.04	2.99	6.37	7.99	7.40	0.05	12.09	11.70
Na_2O	0.01	0.00	0.05	0.05	0.19	0.22	0.37	0.31		8.78	8.45	10.04	8.00	7.32	7.44	0.00	1.07	1.24
K_2O	0.02	0.04	0.03	0.00	9.41	9.68	9.06	9.08		0.08	0.07	0.29	0.07	0.03	0.07	0.06	0.17	0.38
Sum	101.1	99.97	100.7	101.2	95.00	94.91	95.12	94.90		100.4	99.05	99.68	99.14	100.9	100.7	99.46	96.88	96.65
Basis	24 oxygens				22 oxygens					8 oxygens						48 ox	23 ox	
Si	5.86	5.94	5.91	5.99	5.40	5.41	5.42	5.46		2.76	2.74	2.84	2.69	2.62	2.65	7.86	7.00	6.48
Ti	0.01	0.01	0.01	0.00	0.20	0.21	0.17	0.18		0.00	0.00	0.00	0.00	0.00	0.00	0.11	0.03	0.08
Al	4.00	3.93	4.03	4.01	3.43	3.43	3.31	3.23		1.24	1.27	1.15	1.30	1.37	1.34	18.71	1.60	2.18
[β]Fe^{2+}	4.62	5.04	4.30	4.33	2.14	2.14	2.53	2.28		0.01	0.01	0.02	0.01	0.01	0.01	3.30	0.84	1.53
[β]Fe^{3+}					0.11	0.11	0.13	0.12									0.30	0.51
Mn	0.41	0.05	0.81	0.78	0.01	0.01	0.00	0.01		0.00	0.00	0.00	0.00	0.00	0.00	0.01	0.03	0.03
Mg	0.81	0.75	0.68	0.64	2.39	2.32	2.17	2.46		0.00	0.00	0.00	0.00	0.00	0.00	0.66	3.15	2.17
Ca	0.29	0.28	0.25	0.21	0.00	0.00	0.00	0.01		0.24	0.24	0.14	0.31	0.38	0.35	0.00	1.85	1.86
Na	0.00	0.00	0.02	0.02	0.06	0.06	0.11	0.09		0.75	0.73	0.86	0.70	0.63	0.64	0.00	0.30	0.36
K	0.00	0.00	0.00	0.00	1.81	1.87	1.77	1.76		0.00	0.00	0.02	0.00	0.00	0.00	0.02	0.03	0.07
Sum	16.00	16.00	16.00	16.00	15.55	15.56	15.61	15.60		5.00	4.99	5.03	5.01	5.01	5.00	30.66	15.18	15.3
X_{alm}	0.75	0.82	0.71	0.73					X_{ab}	0.76	0.75	0.84	0.69	0.63	0.64			
X_{prp}	0.13	0.12	0.11	0.11					X_{an}	0.24	0.25	0.14	0.31	0.38	0.35			
X_{grs}	0.05	0.05	0.04	0.04					X_{or}	0.00	0.00	0.02	0.00	0.00	0.00			
X_{sps}	0.07	0.01	0.13	0.13														

Total 784 analyses were obtained with the Cameca Camebax SX100 electron microprobe of the Blaise Pascal University in Clermont-Ferrand. Operating conditions included 15 kV accelerating voltage, 10 nA beam current, 1–2 μm beam diameter, 20 s counting time. Standards are natural sillicates (albite, wollastonite, orthoclase, quartz) for calibration of Na, Ca, K, Si, and oxides for calibration of Fe, Mn, Al, Ti, Mg, and Cr. Reported values are averages of three repeated analyses of the same point. Abbreviations: X_{alm} = almandine component, X_{prp} = pyrope component, X_{grs} = grossular component, X_{sps} = spessartine component, X_{ab} = albite component, X_{an} = anorthite component, X_{or} = orthoclase component.

[α] 251: staurolite-bearing unit; 262b and 244: staurolite-free unit; 268a and 252a: amphibole-rich unit.

[β] total Fe expressed as FeO. Fe^{2+} and Fe^{3+} were calculated using the method described in Holland and Blundy (1994).

[γ] spessartine reversal zoning.

[χ] retrograde product.

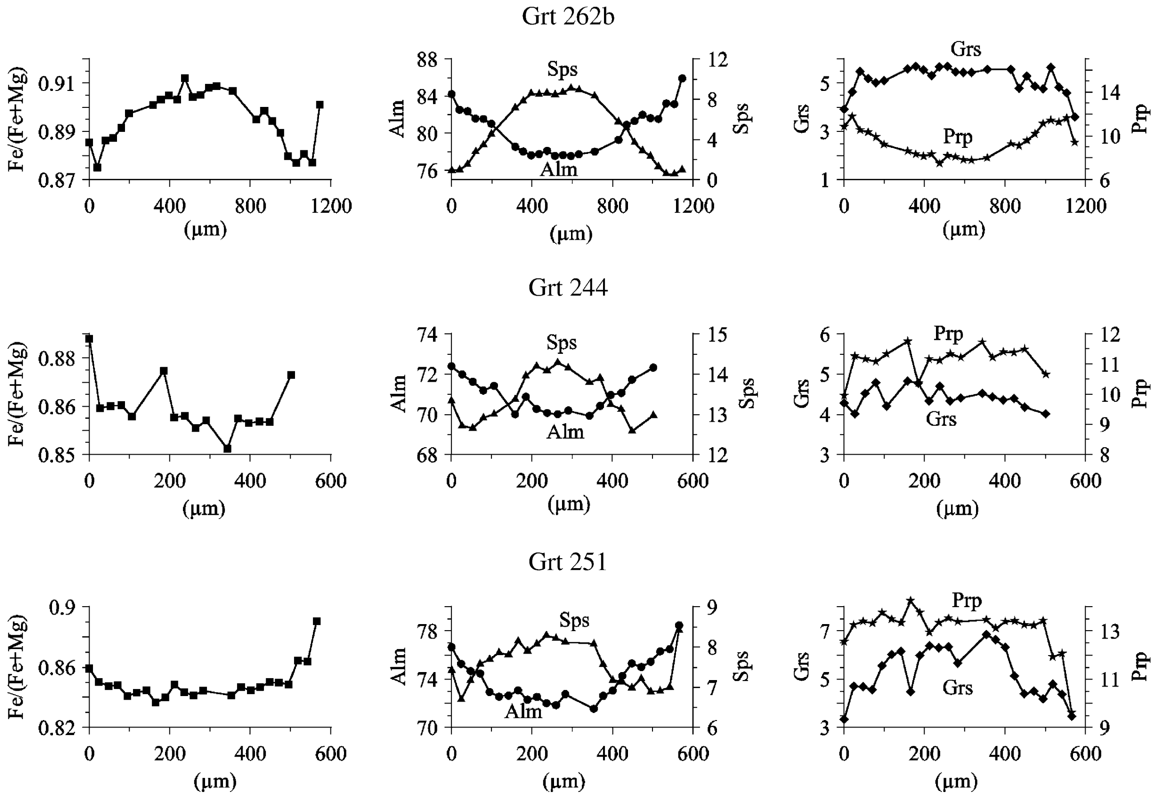

Fig. 7. Compositional zoning of representative garnet crystals. Garnet grains in sample 262b and sample 244 are from the semi-aluminous unit, and garnet in sample 251 from the aluminous unit. Alm $= 100 \times Fe/(Fe^{2+} + Mg + Ca + Mn)$, Prp $= 100 \times Mg/(Fe^{2+} + Mg + Ca + Mn)$, Grs $= 100 \times Ca/(Fe^{2+} + Mg + Ca + Mn)$, Sps $= 100 \times Mn/(Fe^{2+} + Mg + Ca + Mn)$ (abbreviations are from Kretz, 1983).

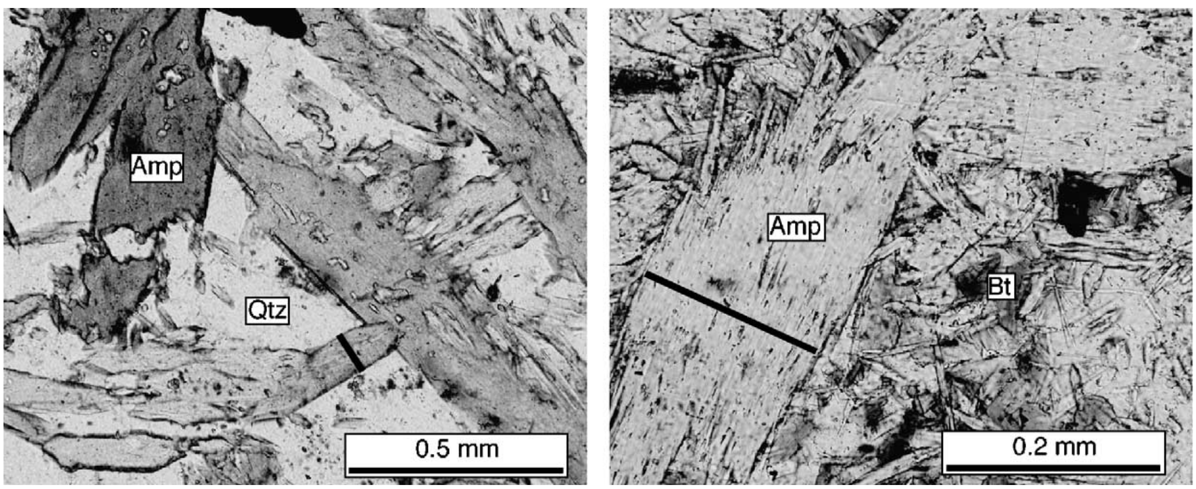

Fig. 8. Photomicrograph showing amphibole crystals in samples 252a (a) and 268a (b). Black lines represent the compositional profiles reported in Figs. 9 and 10.

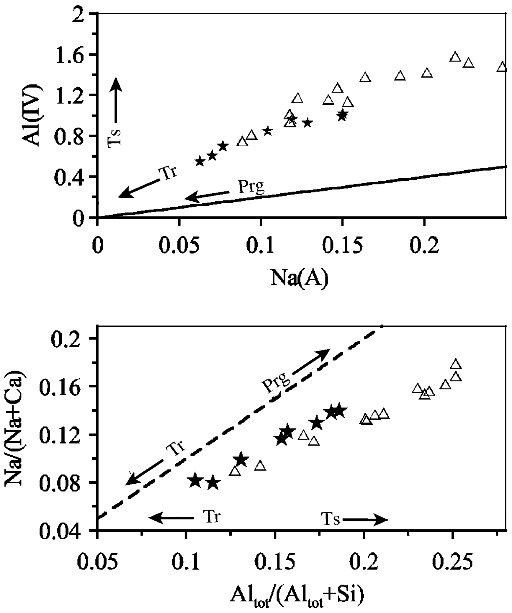

Fig. 9. Compositional profiles of representative amphibole grains in sample 268a (stars) and sample 252a (triangles).

Chl crystallized along the dextral shear planes that formed during the south-southeast compression (D4) and replaces Bt under retrograde greenschist facies conditions.

5.1.3. Amphibole-rich unit

This unit consists of amphibole + Pl + Qtz + Ilm ± Chl ± Tur. Euhedral to subhedral amphibole (0.05–1 mm), the predominant mineral (Fig. 8), does not display a preferred orientation. The amphibole grains plot near the boundary between magnesiohornblende and Tr, following the classification of Leake et al. (1997). They display an array of solid solutions between Tr–Ts and Tr–Prg (Fig. 9), suggesting a typical Act–Hbl exchange reaction (Spear, 1993). Individual grains in sample 268a show an enrichment in Hbl component whereas those in sample 252a show an enrichment of Tr component towards the rims (Fig. 10). The *P–T* evolution corresponding to the zoning pattern will be discussed in Section 5.3.

Pl grains are subhedral to anhedral in shape and range in size from 0.1 to 0.6 mm. They contain inclusions of Qtz and amphibole, and show Ca-increase towards the rims ranging from $An_{0.32}$ to $An_{0.38}$ in sample 252a and from $An_{0.33}$ to $An_{0.52}$ in sample 268a.

5.1.4. The felsic unit

This unit contains Qtz+Pl+Bt+Ilm±Tur. It is similar in texture and mineralogy to the semi-aluminous unit, but this contains higher abundance of quartz than the latter.

5.2. Thermobarometric methods

The felsic unit contains low MnO and TiO_2 contents and feldspar is the only Na- and Ca-bearing phase. Therefore, we used KFMASH petrogenetic grids of Spear and Cheney (1989), together with the aluminosilicate triple point by Richardson et al. (1969) to represent the metamorphic assemblages. We used two Fe–Mg exchange thermometry; Grt–St thermometry of Perchuk (1989) and Grt–Bt thermometry (GARB thermometer) of Pigage and Greenwood (1982) and Williams and Grambling (1990). The classical GARB thermometers of Ferry and Spear (1978) and Indares and Martignole (1985) were not used because Bt compositions in our samples are outside the range accepted for the thermometry (Bt with $(Al^{VI}+Ti)/(Al^{VI}+Ti+Mg+Fe) < 0.15$). Furthermore, the Ti–Al substitution of Bt in our samples is different from Bt used by Indares and Martignole (1985). Pressures were estimated using the Grt–Pl–Sil–Qtz (GASP) barometer of Hodges and Crowley (1985) and Koziol and Newton (1988), and the empirical Grt–Pl–Qtz (GPQ) barometer of Hoisch (1990). We also used the THERMOCALC computer program by Powell et al. (1998) in order to identify possible reactions among given end-member phases and to calculate the pressure and temperature of sub-systems.

The amphibole-bearing rocks contain low TiO_2, MnO, and K_2O and plot on the ACFM + SiO_2 petrogenetic grid defined by Spear (1981). Complementary *P–T* estimates of the amphibole-rich unit were obtained using the thermometer based on the cation exchange reaction of edenite (Holland and Blundy, 1994). Thermobarometers based on the contents of Ti and Al(VI) in amphibole were not used because of the absence of Zo and Ep in our samples (Raase, 1974; Plyusnina, 1982; Hammarstrom and Zen, 1986).

5.3. Metamorphic conditions

5.3.1. Aluminous unit

The KFMASH *P–T* grid of Spear and Cheney (1989) suggests early formation of St at 500–700 °C

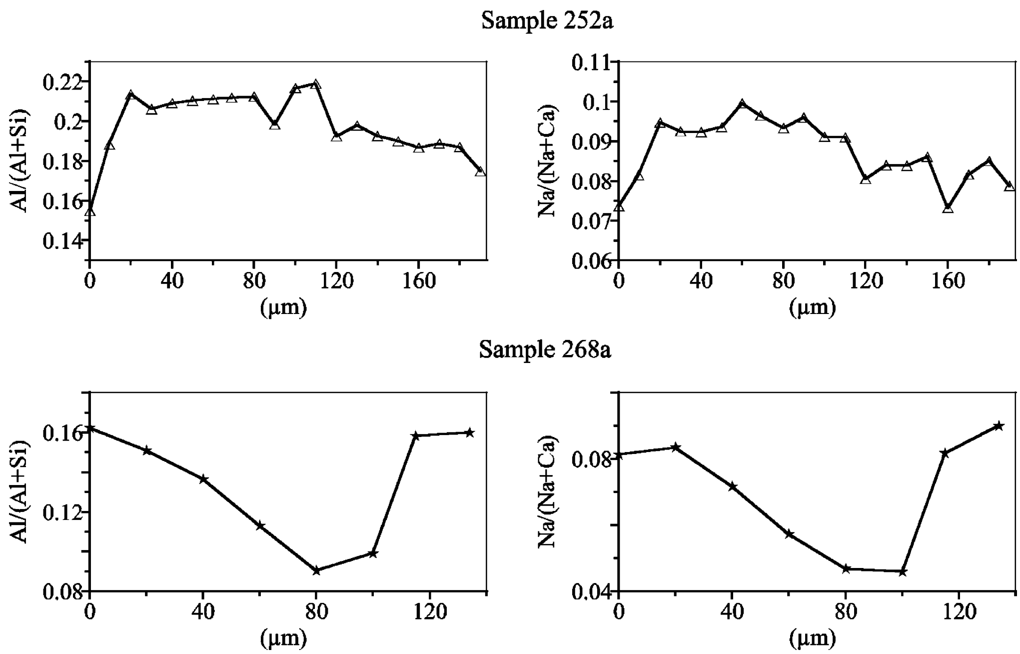

Fig. 10. Compositional zoning of amphibole grains in sample 268a (stars) and sample 252a (triangle) from the amphibole-rich unit. Each profile represents an individual grain from rim to rim through the center of the grain. The grain was selected from four representative grains used for the compositional analysis in each sample. The ratios are atomic.

(Fig. 11). The second metamorphic stage is characterized by the assemblage of Sil + Grt + Bt, suggesting a metamorphic condition on the high temperature side of Reaction 1, greater than 600 °C (Spear and Cheney, 1989; Fig. 11). The absence of Kfs and the occurrence of Sil suggest temperatures lower than 800 °C and pressures between 0.2 and 1 GPa. Sample 251 yielded 628 ± 35 °C and 0.64 ± 0.16 GPa using the THERMOCALC program. Taking the uncertainties into consideration, these results are comparable to the estimated *P–T* based on mineral assemblages (Fig. 11). Furthermore, the values are consistent with the temperature, 600 ± 70 °C, estimated using the GARB thermometer, and also to the 625 ± 50 °C and 0.54 ± 0.09 GPa using the independent GS thermometer and the GASP barometer (Table 3a).

5.3.2. Semi-aluminous unit

The assemblage of Grt + Bt + Pl suggests a metamorphic temperature greater than 500 °C (Spear and Cheney, 1989), as Grt can not crystallise on the low temperature side of the reaction:

$$\text{Fe–Cld} + \text{Ann} + \text{Qtz} = \text{Alm} + \text{Ms} + H_2O \quad (3)$$

In sample 262b, the GARB thermometer and GPQ barometer on Grt cores yielded 610 ± 70 °C and 0.56 ± 0.12 GPa. In sample 244, Grt cores yielded 585 ± 70 °C and 0.71 ± 0.08 GPa, whereas rims with Pl and Bt show a retrograde condition of 540 ± 80 °C and 0.25 ± 0.11 GPa (Table 3b).

5.3.3. Amphibole-rich unit

The absence of clinopyroxene suggests a maximum temperature of 780 °C, following the reaction on the ACFM + SiO_2 petrogenetic grid (Fig. 11; Table 3).

$$\text{Hbl} + \text{Qtz} = 3\text{Cpx} + \text{Pl} + H_2O \quad (4)$$

Metamorphic temperatures are estimated using the Hbl–Pl geothermometer (Holland and Blundy, 1994). Tr commonly crystallizes under greenschist facies condition, whereas Hbl forms under amphibolite facies conditions. Therefore, the zoning from Hbl cores to Tr rims (sample 252a) likely reflects the retrograde path. The Hbl core and co-existing Pl yield a temperature of 700 ± 70 °C.

Amphibole grains without any evidence of retrogression in sample 268a record a prograde path, in-

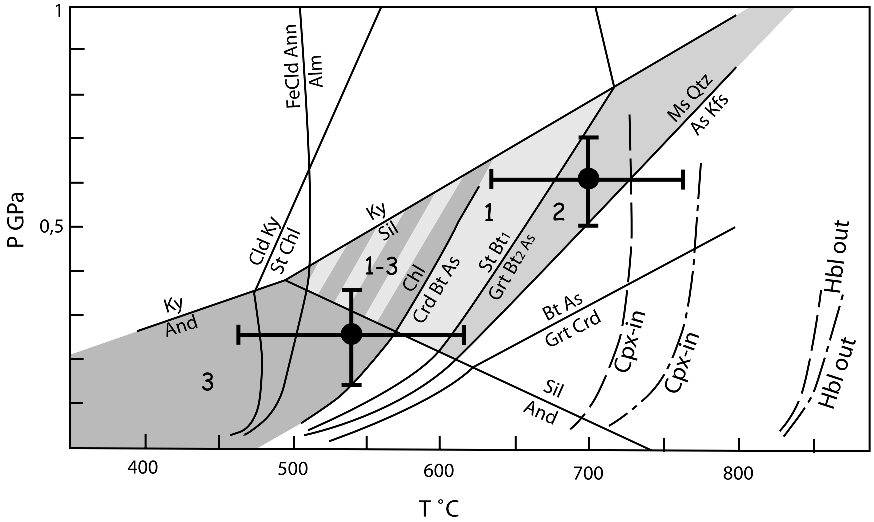

Fig. 11. Solid lines and curves show *P*–*T* grid for pelites in the KFMASH system (modified from Spear and Cheney, 1989). Dash-dot and dashed curves represent the disappearance of Hbl and appearance of Cpx in mafic rocks in the ACFM + SiO_2 system (modified from Spear, 1981). Dash-dot curves are under fo_2 conditions buffered by quartz–fayalite–magnetite and dashed curves under fo_2 conditions buffered by hematite–magnetite. "Cpx" refers to clinopyroxene and other abbreviations of minerals are from Kretz (1983). Shaded fields with 1, 2, and 3 correspond to the *P*–*T* condition based on the mineral assemblages formed during the three tectono-metamorphic events in the Jean Lake area (M1–D1, M3–D3, and M4–D4, respectively; Table 4). Hatched area with 1–3 corresponds to the *P*–*T* stability field where metamorphic assemblages 1 and 3 are both stable. Solid circles are the estimated *P*–*T* values of the M3 and M4 events. Note that the *P*–*T* fields defined by metamorphic mineral assemblages agree well with the *P*–*T* values calculated by mineral assemblages. The error bars represent uncertainties of geothermobarometric calculations (Table 3a and b).

creasing Hbl component towards the rims. The rims yielded a maximum temperature of 600 ± 70 °C using the Hbl–Pl thermometer.

In summary, the rocks in the Jean Lake area underwent a metamorphic event starting with the crystallization of St in the aluminous unit and the increasing Hbl component in amphiboles in the amphibolite unit. The peak metamorphic *P*–*T*, 0.61 ± 0.10 GPa and 700 ± 70 °C, was attained during the D3 regional transpressive deformation. This was followed by retrograde metamorphism forming Chl and Tr during D4 south-southeast compression at 0.25 ± 0.11 GPa, 540 ± 80 °C (LP–MT event).

6. Tectono-metamorphic evolution of the study area and the Quetico belt

The first regional deformation (D1) took place shortly after sedimentation and involved burial of sediments, producing moderate *P*–moderate *T* (MP–MT) metamorphism (Tabor et al., 1989; Pan and Fleet, 1999). This tectono-metamorphic event was followed by mainly strike-slip deformation (D2). This deformation and subsequent deformation (D2–D3) mainly involved strike-slip deformation, implying no significant change in *P* conditions. Therefore, the crystallization of St and Hbl-rich amphiboles under the MP–MT metamorphism in the Jean Lake area occurred before the regional D2 transpressional deformation. It is most likely related to the regional D1.

The second stage of deformation in the Jean Lake area, which corresponds to regional D2–D3, is accompanied by peak metamorphism conditions. The final deformation in the Jean Lake area includes local shearing during south-southeast compression, accompanied by LP–MT metamorphism. The metamorphic condition, 0.25±0.11 GPa and 540±80 °C in the Jean Lake area, is in agreement with the conditions expected from the Subprovince-wide metamorphism. There is a systematic increase in metamorphic conditions, from 0.2 GPa and 500 °C at the USA–Canada border in the west to 0.5–0.6 GPa and 780 °C in the eastern part of the Quetico belt (Pirie and Mackasey, 1978; Percival,

Table 3
(a) Thermobarometric estimates of different lithological units from the Jean Lake area

Unit	Sample	Assemblage	Tr-Ed	P-T Grids$^{\alpha}$	GS$^{\beta}$	GARB$^{\varepsilon}$	GASP$^{\psi}$	GPQ$^{\varepsilon}$	THERMOCALC$^{\phi}$	
			T(°C)$^{\delta}$	T(°C), P (Gpa)	T(°C)$^{\delta}$	T (°C)$^{\delta}$	P (GPa)$^{\eta}$	P (GPa)$^{\eta}$	T (°C)	P (GPa)
St-free	244	Grt + Bt + Pl				585 ± 70 [n=4]		0.71 ± 0.08 [n=1]	Insufficient phases	Insufficient phases
St-free	262b	Grt + Bt + Pl		stable Grt > 500		610 ± 70 [n=5]		0.56 ± 0.12 [n=6]	Insufficient phases	Insufficient phases
St-bearing	251	Grt + Bt +Pl + Sil + St		St => Sil+Grt+Bt T > 650, 0.45 < P Ky absence T< 800, 0.9 > P	625 ± 50 [n=6]	600 ± 70 [n=6]	0.59 ± 0.11 [n=3]	0.54 ± 0.09 [n=3]	628 ± 35 sidfit=0.28	0.64 ± 0.16 sidfit=0.28
Amp-rich	252a	Amp + Pl	700 ± 70 [n=3]	Cpx absence <780					Insufficient phases	Insufficient phases
Amp-rich	268a	Amp + Pl	600 ± 70 [n=5]						Insufficient phases	Insufficient phases
Best estimates of the peak metamorphism$^{\gamma}$						*P = 0.61 ± 0.10 GPa, T = 700 ± 70°C*				

(b) Thermobarometric estimates of the LP-HT metamorphism of the Jean Lake area

Unit	Sample	Assemblage	Tr-Ed	P-T Grids$^{\beta}$	GS$^{\delta}$	GARB$^{\varepsilon}$	GASP$^{\psi}$	GPQ$^{\varepsilon}$	THERMOCALC$^{\phi}$	
						T°C$^{\delta}$		P (GPa)$^{\eta}$	T°C	GPa
St-free	244	Grt + Bt + Pl				540 ± 80 [n=4]		0.25 ± 0.11$^{\eta}$ [n=3]	Insufficient phases	Insufficient phases

n: the number of mineral pairs used for the calculations is in parentheses.
α: the grid by Spear and Cheney (1989).
β: Garnet–staurolite thermometer (Perchuk, 1989).
δ: Uncertainty considers the discrepancy of the calculated results among different pairs and the uncertainties (at 2σ-level) related to the equation given by the authors of the original papers.
η: Uncertainties in pressure estimates correspond to the standard deviation (2σ) with the average previously calculated temperature.
ε: Garnet–plagioclase–quartz geobarometers (Hoisch, 1990).
ψ: Garnet–aluminosilicate–silica–plagioclase geobarometer (Hodges and Crowley, 1985; Koziol and Newton, 1988).
ϕ: THERMOCALC computer program (Powell et al., 1998).
γ: pressure is an average of all estimates and the temperature is that of the sample 252a using the Tr-Ed thermometer.
Abbreviations: Amp = amphibole, Bt = biotite, Cpx = clinopyroxene, Grt = garnet, Kfs = K-feldspar, Ky = kyanite, Pl = plagioclase, Sil = sillimanite, St = staurolite, Tr = tremolite.

Table 4
Timing of sedimentation, deformation (*D*) and metamorphism in the Quetico metasedimentarybelt

Events	Previous studies	This study	Proposed timing
Sedimentation	2698 to <2690 Ma (1,2)		2698 to <2690 Ma
D1			2698–2689 Ma
D2	2689–2684 Ma (3), ? to < 2666 Ma (4)		2689–2684 Ma
D3			2684–2671 Ma
D4		2667 ± 20 Ma	2671–2667 Ma
MP–MT metamorphism (M1)		Synchronous with D1	
Peak of metamorphism (M3)		Synchronous with D3	
LP–MT metamorphism (M4)	2671–2667 Ma (5), synchronous with D2 (4)	Synchronous with D4	

References: (1) Davis et al. (1990); (2) Zaleski et al. (1999); (3) Percival (1989); (4) Pan et al. (1998); (5) Percival and Sullivan (1988).

1989). Greenschist facies retrograde metamorphism is recorded at the end of D4 deformation in the Jean Lake area. Similar retrograde metamorphism is observed in many other places in the Quetico belt (Percival, 1989; Pan et al., 1994; Pan and Fleet, 1999). The D3 and D4 are described in Sawyer (1983) and Williams (1991).

The timing of these deformation events and their relationships with regional metamorphism are in debate. Percival (1989 and references therein) suggested that regional D2 deformation is bracketed between 2689 and 2684 Ma and the LP–MT event between 2671 and 2667 Ma based on ages of intrusive rocks and detailed structural study in Shebandowan and adjacent Quetico belt (Fig. 2). Pan et al. (1998) proposed a much later date for the regional D2 based on 2666 ± 1 Ma pegmatitic rocks concordant to the penetrative S2 foliation. This would imply that the D2 deformation occurred during the regional metamorphism dated at 2670–2650 Ma (Percival, 1989). This is not consistent with our data from the Jean Lake area, where the LP–MT metamorphism was synchronous with the D4 deformation. To confirm this time relationship, we dated monazite that crystallized during the LP–MT metamorphic stage (D4).

7. Dating of monazite

Thirty-six grains of monazite were examined in sample 251. Monazite shows no compositional zoning, contains high U (up to 0.8 wt.%), Th (up to 5 wt.%), and light rare earth elements (REE). Chondrite-normalized REE patterns of all grains are similar, suggesting a single generation of monazite

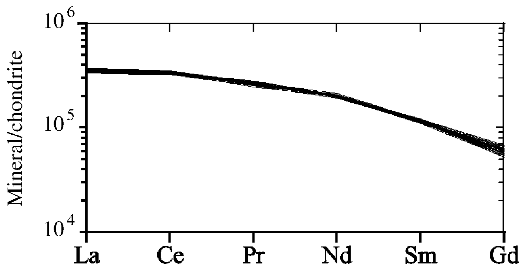

Fig. 12. Chondrite-normalized REE patterns of 34 monazite grains from the aluminous unit of quartzo-feldspathic rocks (sample 251). The REE contents were determined using a Camebax electron microprobe, with an accelerating voltage of 15 kV, and a beam current of 100–150 nA. The counting times were 20 s for Sm and Gd, 15 s for Pr and Nd, and 10 s for La and Ce. The standard is a synthetic phosphate. Relative errors are 5% for La and Ce, 20% for Nd and Pr, 40% for Sm and Gd.

(Fig. 12). The age was calculated from the concentration of U, Th, and Pb assuming no Pb at the time of crystallization following the method of Montel et al. (1996) (see caption for Fig. 13). The calculated mean age is 2667 ± 20 Ma with a mean square of weighted deviates (MSWD) of 0.36. The error is estimated following the method described in Montel et al. (1996). The narrow range of MSWD supports a single generation population of monazite in the sample (Fig. 13).

8. Discussion

8.1. Pressure–temperature–time path

The age of 2667 ± 20 Ma for the D4 and LP–MT metamorphism is in good agreement with the time

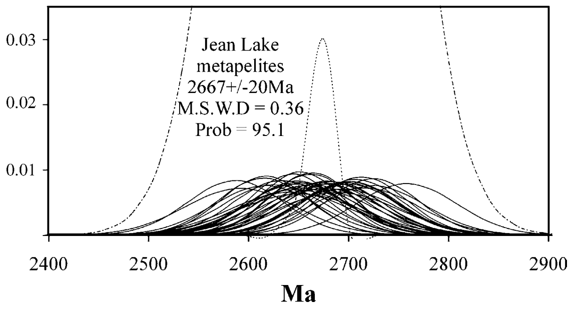

Fig. 13. Weighted histogram of the age of monazite. The age (t) is calculated from the U, Th, and Pb concentrations of the sample, assuming that Pb is a radiogenic decay product.

$$\mathrm{Pb} = \frac{\mathrm{Th}}{232}[\exp(\lambda_t^{232}) - 1]208 + \frac{\mathrm{U}}{238.04}0.9928[\exp(\lambda_t^{238}) - 1]206 + \frac{\mathrm{U}}{238.04}0.0072[\exp(\lambda_t^{235}) - 1]207$$

where Pb, U, Th are their concentration, and λ^{232}, λ^{235}, λ^{238} are the decay constants of ^{232}Th, ^{235}U, ^{238}U, respectively. The mean age was estimated from a least-squares approach considering errors of the measured concentrations of U, Th, and Pb at the 95% level. Each measurement is represented by its probability density function. Note that there is no unit for the vertical scale because the integration of these factors on time yields a constant (Montel et al., 1996). The dash curve is computed with the program Final4 (Montel et al., 1996) and the dash-dot line represents the sum of all curves. The U, Th, and Pb contents were determined using a Camebax electron microprobe, with an accelerating voltage of 15 kV and beam current of 100–150 nA. The counting times for peak/background were 300 s/100 s for Pb, 50 s/20 s for U, and 40 s/20 s for Th. The standards are uraninite (U), Th oxide (Th), and a synthetic glass (Pb).

span of 2671–2667 Ma suggested by Percival and Sullivan (1988) and 2668 ± 6 Ma of the U–Pb age of metamorphic titanite reported by Pettigrew et al. (2001). For the D2 deformation, we adopt 2689–2684 Ma as suggested by Percival (1989). The pegmatites of 2666 ± 1 Ma dated by Pan et al. (1998) likely intruded along the pre-existing S2 foliation.

Combining our data with those of previous workers, we propose the following *P–T–t* path for the central part of the Quetico metasedimentary. The rocks were buried to develop a MP–MT mineral assemblage formed under amphibolite facies conditions during the D1 shortly after the sedimentation bracketed between 2698 and <2690 Ma (Zaleski et al., 1999). Transpressive deformation (D2–D3) started at 2689 Ma and was accompanied by peak metamorphic conditions of $P = 0.61 \pm 0.10$ GPa and $T = 700 \pm 70\,^{\circ}$C. The subsequent south-southeast compression, D4, was accompanied by east–west lateral extrusion under LP–MT metamorphic conditions (0.25 ± 0.11 GPa, 540 ± 80 °C) at 2671–2667 Ma (Fig. 14). This deformation likely continued under retrograded greenschist-facies conditions, forming lineations of Chl and Tr.

8.2. Tectonic setting of the sedimentation of the Quetico belt

A variety of tectonic settings have been proposed for the deposition of the sediments in the Quetico belt. We briefly present the evidence for and against several possible settings.

8.2.1. Ensialic basin

Given the elongate shape of the Quetico metasedimentary belt, an aborted rift basin in sialic crust was proposed by Percival (1989). However, as discussed by Percival (1989) and Williams (1990), the turbiditic character of the Quetico sedimentary rocks is markedly different from alluvial conglomeratic sequences that commonly develop in a continental extensional basin.

8.2.2. Back-arc basin or intra-arc basin

The evidence against this model is essentially the same as for the ensialic rift environment described above. In addition, the Quetico belt does not contain rift-related mafic igneous rocks that are common in a back-arc or intra-arc basin.

8.2.3. Forearc setting

This was first suggested by Devaney and Williams (1988) based on a sedimentological-structural study in the Beardmore–Geraldton area (Fig. 2) in the southern margin of the Wabigoon Subprovince. They outlined north-dipping thrust slices of volcanic-sedimentary rocks and interpreted the area as a forearc basin in an accretion model. Sediments in modern forearc basins are thin (Lallemand, 1999), which is not consistent with the observed 20 km of burial corresponding to MP–MT metamorphism shortly (<9 My) after sedimentation.

8.2.4. Accretionary prism

This model, proposed by Percival (1989) and Williams (1990), suggests that submarine fans and abyssal turbidites were first deformed during their

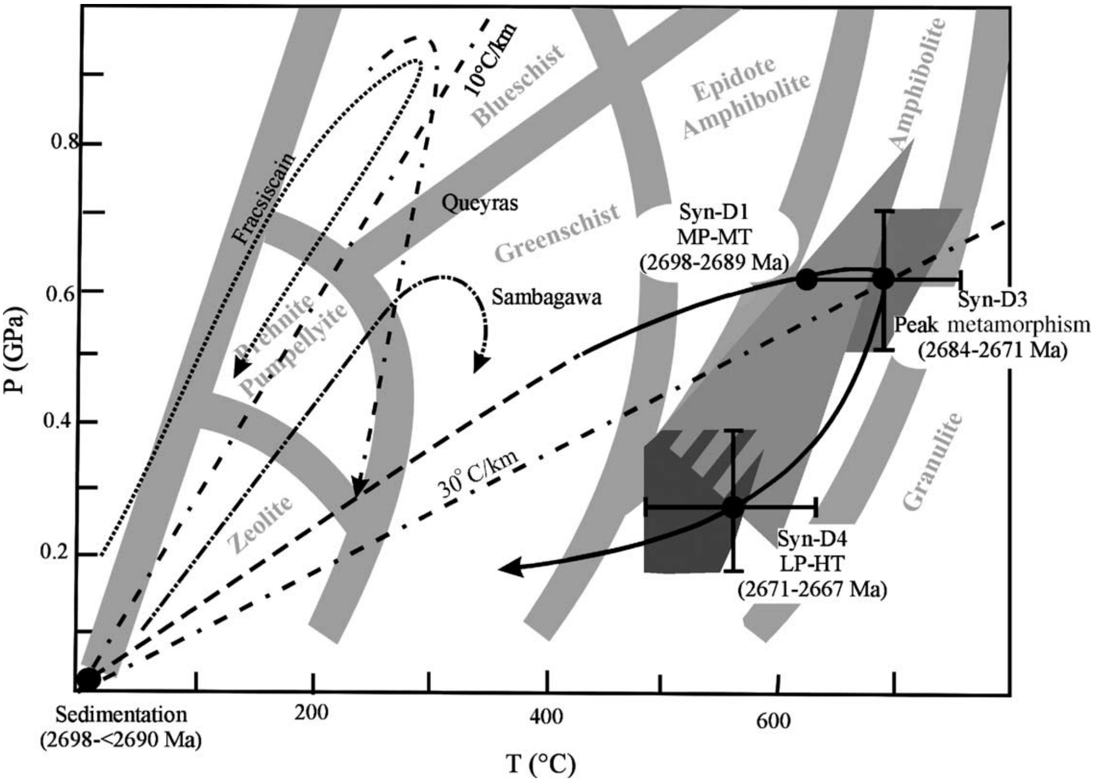

Fig. 14. Estimated *P*–*T*–*t* path (solid curve) for the rocks in the Jean Lake area compared to the paths of modern accretionary prisms. Queyras (Schwartz et al., 2000), Sambagawa (Ernst, 1988), and Franciscan (Ernst, 1988). Solid circles with error bars are *P*–*T* values estimated using thermobarometeric calculations. The metamorphic facies shown by thick light gray curves are from Spear (1993). Dot-double-dash lines represent two geothermal gradients; 10 and 30 °C/km. Shaded areas are the intersections between *P*–*T* stability area derived from mineral assemblages (see Fig. 11), and *P*–*T* estimated from thermobarometric calculations (solid circles).

accretion onto the active Wabigoon arc (D1) and later during the docking of the Wawa arc from the south (D2–D3).

This model is compatible with the observed deformation and MP–MT metamorphism shortly after sedimentation. Burial of sediments up to 0.6 ± 0.1 GPa in less than 9 My is observed in modern subduction zones, such as Sambagawa belt in Japan, where sediments were buried to similar depths in less than 1 My (Enami, 1998; Inui and Toriumi, 2002; Aoya et al., 2003). Furthermore, the younging age of sedimentation toward the south in the Quetico belt (Zaleski et al., 1999) is compatible with a southward propagation of the active front in a north dipping subduction as shown by Platt (1986). An oblique component of the convergence in the Quetico belt likely contributed to the transpressional structures, dextral wrench zones, and transcurrent faults along subprovince boundaries. The late LP–MT metamorphism is explained by thermal relaxation after cessation of subduction.

Seismic reflection profile from the Superior Province illustrates north-dipping crust and the remnant of the subducted lithosphere down to 80–100 km in the mantle (Ludden et al., 1993; Calvert et al., 1995). Island arcs were continuously accreted to a continent to the north through subduction of intervening oceanic crust and collision. The development of the Superior Province is very similar to modern tectonic processes. This is further supported by petrological and structural studies in the Superior Province (Desrochers et al., 1993; Tomlinson et al., 1996; Davis, 1998).

The proposed interpretation, Phanerozoic style plate tectonics in Archean time, has been challenged by

Hamilton (1998) based on the lack of blueschist, ophiolite complexes, and tectonic mélanges of accretionary prisms. The absence of blueschist is explained by higher temperature gradients in accretionary prisms in Archean. Upper sections of ophiolitic rocks have been identified in Archean terranes including those in Canadian Shield (Card, 1990; Tomlinson et al., 1996). It is likely that Archean oceanic lithosphere was thick due to hotter mantle temperatures and that only upper sections of oceanic plates could have been delamination and obducted (Hoffman and Ranalli, 1988).

Modern accretionary prisms commonly contain highly deformed tectonic mélange. For example, a mélange unit of the Shimanto accretionary prism in Japan includes slivers of basaltic pillow lavas, shales, and volcanic ash layers, in association with highly sheared argillaceous sedimentary rocks of turbidites (Taira, 1981; Taira et al., 1988, 1992, 1997). Similar assemblages of highly tectonic rocks are reported in the Quetico belt, although they are not identified as tectonic mélange units. For example, Williams (1989) reported the occurrence of thin sheets of gabbro, tonalite, granodiorite, and ultramafic to anorthositic rocks interbedded with tectonized turbiditic sedimentary rocks. On the southern side of the Quetico belt, blocks (gabbro, rhyolite, tonalite, and volcanic rocks) in a mylonitic sedimentary matrix were also reported and identified as part of a mélange unit by Polat et al. (1998) and Polat and Kerrich (1999).

Thus, we suggest that an accretionary prism setting best explains the sedimentologic, metamorphic, tectonic and geophysics characteristics of the Quetico belt.

8.3. Source and evolution of the Quetico accretionary prism

The sedimentary rocks in the Jean Lake area formed by mixing of quartzo-feldspathic rocks and komatiitic basalts, three types of geological setting are considered for the komatiitic basalts: an oceanic island that accreted to the Quetico belt, igneous rocks in the Quetico belt, and the adjacent southern Wabigoon Subprovince. An accreted oceanic island and a volcano inside the Quetico belt are unlikely simply because there are no komatiites or komatiitic basalts in the Quetico belt. There are abundant mafic igneous rocks in the southern Wabigoon Subprovince that are contemporaneous with the sedimentation of the Quetico sediments. They include a suite of sanukitoids of ∼2690 Ma in the Wabigoon Subprovince (Stern and Hanson, 1991; Stevenson et al., 1999), and voluminous mafic–ultramafic rocks ∼2692 Ma in the southern Wabigoon belt along the boundary with the Quetico belt (Sutcliffe et al., 1989; Blackburn et al., 1991; Pettigrew and Hattori, 2002).

High contents of MgO and CaO suggest a proximal source, since these elements are easily leached during weathering and transportation (Nesbitt and Young, 1989). Immature sediments may be formed during sudden uplift and erosion of a source terrane, or by discharge of pyroclastic material from a volcano, but the Jean Lake is located more than 100 km from the southern Wabigoon Subprovince. The mafic sedimentary rocks are too immature to be transported for such a long distance from the source. This problem may be explained by lateral transport of sediments during the development of accretionary prisms.

In modern accretionary prisms, sediments are thickened through repeated underplating and near-horizontal thrusting (Cloos, 1986; Platt, 1986; Cloos and Shreve, 1988; Lallemand, 1999; Hashimoto and Kimura, 1999). Underplating at the base of the wedge is compensated by extension in the shallow part of the wedge, resulting in lateral transport of sediments away from the wedge toward the prism front (Platt, 1986; Lallemand, 1999; Fig. 15).

In the Quetico belt, sediments would have been moved southward, and buried during the development of the accretionary prism (Fig. 15). We suggest that the rocks in the Jean Lake area were originally deposited close to the Quetico–Wabigoon boundary, displaced towards the south, and buried up to ∼20 km by rapid underthrusting along a MP–MT metamorphic gradient to amphibolite facies conditions during the D1 deformation.

Subsequent dextral transpressive deformation (D2–D3) displaced the sedimentary rocks to the west from the original depositional site. The dextral component during D2–D3 was likely caused by strain partitioning in an oblique convergent system as described in many modern subduction zones, such as the Ryukyu, Higurangi, Aleutian, and western North American subduction zones (Lallemand, 1999). The rocks were then uplifted during the D4 deformation. This exhumation was likely accompanied by the de-

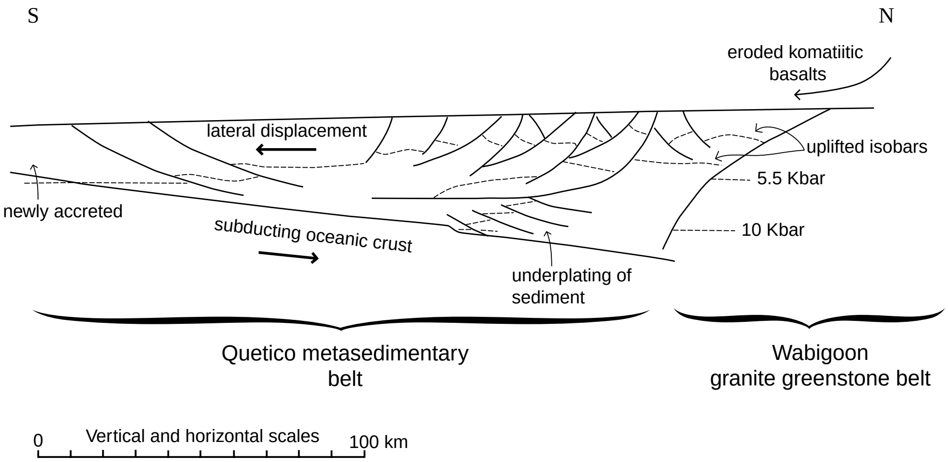

Fig. 15. Schematic model showing the evolution of the Quetico accretionary prism based on the general model presented by Platt (1986). Thick arrows show the direction of movement.

velopment of LP–MT metamorphism and voluminous granitic plutonism. This has been interpreted previously as a result of thermal relaxation (Percival, 1989; Williams, 1991).

8.4. Comparison with modern subduction zones

Our data suggest the burial of sedimentary rocks to a depth of about 20 km and their metamorphism up to amphibolite facies conditions in less than 9 My, and their exhumation up to LP–MT conditions within about 15 My. The burial and exhumation rates are comparable with those of Phanerozoic terranes. The typical burial rate of sediments in Phanerozoic prisms is about 3–8 cm per year (Demets et al., 1990) and their exhumation rate is about 0.2–1 mm per year (Duchêne et al., 1997; Schwartz et al., 2000; DeSigoyer et al., 2000). Using these burial and exhumation rates, our *P–T* path suggests that the Quetico rocks would have been buried in less than ∼1 My and exhumed within 12–60 My. Comparable burial and exhumation rates of the Quetico belt with those from modern subduction zones suggest that the Neoarchean tectonic regime was essentially similar to the modern analogs.

Modern subduction zones commonly contain HP–LT metamorphic rocks, such as blueschists and eclogites. They formed under low geothermal gradients, ∼10 °C/km (Fig. 14; Ernst, 1988; Ernst and Liou, 1999; Schwartz et al., 2000). Like many other Archean sedimentary terranes, the Quetico belt does not contain HP–LT rocks. The lack of such metamorphic rocks in Archean terranes has been in debate (e.g. De Wit, 1998). This may be attributed to high geothermal gradients (∼30 °C/km) during Archean time possibly caused by local effects such as magma emplacement and ridge subduction, as proposed to account for high geothermal gradients of several Phanerozoic accretionary prisms (Sakaguchi, 1999). Upwelling of magmas may be supported by the occurrence of small, yet numerous intrusions in the belt including 2680 ± 1 Ma alkaline igneous rocks (Hattori and Percival, 1999).

9. Conclusion

Our study in the Jean Lake area in the central Quetico belt shows the mafic rocks formed by sedimentary process with a contribution of komatiitic basalts, that were likely exposed on the southern Wabigoon Subprovince in late Archean time. The tectono-metamorphic evolution recorded by these rocks suggests that the Quetico sedimentary rocks formed in an accretionary prism above a north-dipping subduction slab beneath the Wabigoon Subprovince. Our proposed interpretation is suggested by a rapid burial of sediments (less than 9 My) down to amphibolite facies conditions (0.6 ± 0.1 GPa and 700 ± 70 °C), followed by exhumation under regional compressive deformation in about 15 My. This *P–T–t* evolution is comparable to those of modern accretionary prisms. During their burial, the temperature gradient recorded was around 30 °C/km which is significantly higher than modern counterparts (10 °C/km). The lack of HP–LT rocks, such as blueschists, in the Quetico belt is attributed to such high geothermal gradients.

Acknowledgements

We thank G. Mahéo and P. Goncalves for discussions, B. Lassen, N.T. Pettigrew, and P. Chantigny for discussions and assistance in the field, M. Veschambre of Blaise Pascal University in Clermont-Ferrand for his technical assistance with the electron microprobe, Ron Hartree and Monika Wilk-Alemany of the University of Ottawa for XRF and trace element analysis, and George Mrazek of the University of Ottawa and M. Clermont of the University of Lyon1 for making thin sections. We thank John A. Percival, Ralph Kretz, Flemming Mengel, J. Martignole, and M. Van Kranendonk for their helpful comments.

References

Aoya, M., Uehara, S., Matsumoto, M., Wallis, S.R., Enami, M., 2003. Subduction-stage pressure–temperature path of eclogite from the Sambagawaa belt: prophetic record for oceanic-ridge subduction. Geology 31 (12), 1045–1048.

Ayer, J.A., 1999. Petrogenesis and Tectonic Evolution of the Lake of the Woods Greenstone Belt, Western Wabigoon Subprovince, Ontario, Canada. Unpublished Ph.D. thesis. University of Ottawa, Canada, 207 pp.

Ballantyne, P., 1992. Petrology and geochemistry of the plutonic rocks of the Halmahera ophiolite, eastern Indonesia, an analogue of modern oceanic forearcs. In: Parson, L.M., Murton, B.J., Browning, P. (Eds.), Ophiolites and Their Modern Oceanic Analogues. Geological Society Special Publication No. 60. pp. 179–202.

Blackburn, C.E., Johns, G.W., Ayer, J., Davis, D.W., 1991. Wabigoon Subprovince. In: Thurston, P.C., Williams, H.R., Sutcliffe, R.H., Stott, G.M. (Eds.), Geology of Ontario. Ontario Geological Survey Special Vol. 4. Ontario Geological Survey, Ontario, Canada, pp. 303–381.

Calvert, A.J., Sawyer, E.W., Davis, D.W., Ludden, J.N., 1995. Archean subduction inferred from seismic image of a mantle suture in the Superior Province. Nature 375, 670–674.

Card, K.D., 1990. A review of the Superior Province of the Canadian Shield, a product of Archean accretion. Precambrian Res. 48, 99–156.

Cloos, M., 1986. Bluechists in the Franciscan complex of California; petrotectonic constraints on uplift mechanisms. Memoir—Geol. Soc. Am. 164, 77–93.

Cloos, M., Shreve, R.L., 1988. Subduction channel model of prism accretion, mélange formation, sediment subduction, and subduction erosion at convergent plate margins; part II, implications and discussion. Pure Appl. Geophys. 128 (3–4), 501–545.

Cook, F.A., Van der Velden, A.J., Hall, K.W., Roberts, B.J., 1999. Frozen subduction in Canada's Northwest Territories: lithoprobe deep lithospheric reflection profiling of the western Canadian Shield. Tectonics 18, 1–24.

Davis, D.W., Pezzutto, F., Ojakangas, R.W., 1990. The age and provenance of metasedimentary rocks in the Quetico Subprovince, Ontario, from single zircon analyses: implications for Archean sedimentation and tectonics in the Superior Province. Earth Planet. Sci. Lett. 99, 195–205.

Davis, D.W., 1998. Speculation on the formation and crustal structure of the Superior Province from U–Pb geochronology. In: Helmstaedt, H., Harrap, R. (Eds.), Western Superior Lithoprobe 1998 Annual Meeting: Progress Reports, Technical Communications, and Abstracts. University of British Colombia, Lithoprobe Secretariat (for the) Canadian Lithoprobe Program, Vancouver, BC, Canada, pp. 21–28.

Demets, C., Gordon, R.G., Argus, D.F., Stein, S., 1990. Current plate motions. Geophys. J. Int. 101, 425–478.

De Sigoyer, J., Chavagnac, V., Blichert-Toft, J., Villa, I.M., Luais, B., Guillot, S., Cosca, M., Mascle, G., 2000. Dating the Indian continental subduction and collisional thickening in the northwest Himalaya: multichronology of the Tso Morari eclogites. Geology 28, 487–490.

Desrochers, J.P., Hubert, C., Ludden, J.N., Pilote, P., 1993. Accretion of Archean oceanic plateau fragments in the Abitibi greenstone belt, Canada. Geology 21, 451–454.

Devaney, J.R., Williams, H.R., 1988. Evolution of an Archean Subprovince boundary: a sedimentological and structural study of part of the Wabigoon–Quetico boundary in northern Ontario, Canada. J. Earth Sci. 26, 1013–1026.

De Wit, M.J., 1998. On Archean granites, greenstones, cratons and tectonics: does the evidence demand a verdict? Precambrian Res. 91, 181–226.

Duchêne, S., Lardeaux, J.M., Albarède, F., 1997. Exhumation of eclogites: insights from depth–time path analysis. Tectonophysics 280, 125–140.

Enami, M., 1998. Pressure–temperature path of Sambagawa prograde metamorphism deduced from grossular zoning of garnet. J. Metamorph. Geol. 16, 97–106.

Ernst, W.G., 1988. Tectonic history of subduction zones inferred from retrograde blueschist P–T paths. Geology 16, 1081–1084.

Ernst, W.G., Liou, J.G., 1999. Overview of UHP metamorphism and tectonics in well-studied collisional orogens. Int. Geol. Rev. 41, 477–493.

Ferry, J.M., Spear, F.S., 1978. Experimental calibration of the partitioning of Fe and Mg between biotite and garnet. Contrib. Mineral. Petrol. 66, 113–117.

Fralick, P.W., Kronberg, B.I., 1997. Geochemical discrimination of clastic sedimentary rock sources. Sediment. Geol. 113, 111–124.

Fralick, P.W., Wu, J., Williams, H.R., 1992. Trench and slope basin deposits in an Archean metasedimentary belt, Superior Province, Canadian Shield. Can. J. Earth Sci. 29, 2551–2557.

Fryer, P., Ambos, E.L., Hussong, D.M., 1995. Origin and emplacement of Mariana forearc seamounts. Geology 13, 774–777.

Hamilton, W.B., 1998. Archean magmatism and deformation were not products of plate tectonics. Precambrian Res. 91, 143–179.

Hammarstrom, J.M., Zen, E.-An., 1986. Aluminum in hornblende: an empirical igneous geobarometer. Am. Mineral. 71, 1297–1313.

Hashimoto, Y., Kimura, G., 1999. Underplating processes from melange formation to duplexing; example from the Cretaceous Shimanto belt, Kii Peninsula, Southwest Japan. Tectonics 18, 92–107.

Hattori, K.H., Percival, J.A., 1999. Archean carbonate-bearing alkaline igneous complexes of the western Quetico metasedimentary belt, Superior Province, Ontario, Geol. Surv. Can. Curr. Res. C, pp. 221–231.

Hodges, K.V., Crowley, P.D., 1985. Error estimation and empirical geothermobarometry for pelitic systems. Am. Mineral. 70, 702–709.

Hoffman, P.F., Ranalli, G., 1988. Archean oceanic flake tectonics. Geophys. Res. Lett. 15, 1077–1080.

Hoisch, T.D., 1990. Empirical calibration of six geobarometers for the mineral assemblage Qtz + muscovite + biotite + plagioclase + garnet. Contrib. Mineral. Petrol. 104, 225–234.

Holland, T., Blundy, J., 1994. Non-ideal interactions in calcic amphiboles and their bearing on amphibole-plagioclase thermometry. Contrib. Mineral. Petrol. 116, 433–447.

Indares, A., Martignole, J., 1985. Biotite–garnet geothermometry in the granulite facies: the influence of Ti and Al in biotite. Am. Mineral. 70, 272–278.

Inui, M., Toriumi, M., 2002. Prograde pressure–temperature paths in the pelitic schists of the Sambagawa metamorphic belt, southwest Japan. J. Metamorph. Geol. 20, 563–580.

Koziol, A.M., Newton, R.C., 1988. Redetermination of the anorthite breakdown reaction and improvement of the plagioclase–garnet–Al_2SiO_5–Qtz geobarometer. Am. Mineral. 73, 216–223.

Kretz, R., 1983. Symbols for rock-forming minerals. Am. Mineral. 68 (1–2), 277–279.

Lallemand, S., 1999. La Subduction Océanique. Gordon and Breach Science Publishers, Amsterdam, 193 pp.

Lassen, B., Hattori, K., Percival, J.A., 2000. Late Archean alkaline magmatism in the western Quetico belt, Superior Province, Ontario. Geol. Surv. Can. Curr. Res. C21, 6.

Leake, B.E., Woolley, A.R., Birch, W.D., Gilbert, M.C., Grice, J.D., Hawthorne, F.C., Kato, A., Kisch, H.J., Krivovichev, V.G., Linthout, K., Laird, J., Mandarino, J., Maresch, W.V., Nickel, E.H., Rock, N.M.S., 1997. Nomenclature of amphiboles. Report of the Subcommittee on Amphiboles of the International Mineralogical Association Commission on New Mineral Names. Eur. J. Miner. 9, 623–651.

Ludden, J.N., Hubert, C., Barnes, A., Milkereit, B., Sawyer, E., 1993. A three dimensional perspective on the evolution of Archean crust: LITHOPROBE seismic reflection images in the southwestern Superior Province. Lithos 30, 357–372.

Montel, J.M., Veschambre, S.F.M., Nicollet, C., Provost, A., 1996. Electron microprobe dating of monazite. Chem. Geol. 131, 37–53.

Nesbitt, H.W., Young, G.M., 1989. Formation and diagenesis of weathering profiles. J. Geol. 97, 129–147.

Nicolas, A., 1989. Structures and Dynamics of Oceanic Lithosphere. Klüwer Academic Publishers, New York, 188 pp.

Ojakangas, R.W., 1985. Review of Archean clastic sedimentation, Canadian Shield: major felsic volcanic contributions to turbidite and alluvial fan–fluvial facies associations. In: Ayres, L.D., Thurston, P.C., Card, K.D., Weber, W. (Eds.), Evolution of Archean Supracrustal Sequences. Geol. Assoc. Can. Spec. Paper 8, pp. 23–48.

Ontario Geological Survey, 1991. Bedrock Geology of Ontario, west-central sheet; Ontario Geological Survey, Map 2542 (scale of 1:1 000 000).

Pan, Y., Fleet, M.E., 1999. Kyanite in the western Superior Province of Ontario: implication for Archean accretionary tectonics. Can. Miner. 37, 359–373.

Pan, Y., Fleet, M.E., Williams, H.R., 1994. Granulite–facies metamorphism in the Quetico Subprovince, north of Manitouwadge, Ontario. Can J. Earth Sci. 31, 1427–1439.

Pan, Y., Fleet, M.E., Heaman, L., 1998. Thermo-tectonic evolution of an Archean accretionary complex: U–Pb geochronological constraints on granulites from the Quetico Subprovince, Ontario, Canada. Precambrian Res. 92, 117–128.

Perchuk, L.L., 1989. Internal consistency of some Fe–Mg geothermometers based on Nernst law, a revision (in Russian, with English Abstract). Geokhimiya 5, 611–622.

Percival, J.A., 1989. A regional perspective of the Quetico accretionary complex, Superior Province, Canada. Can. J. Earth Sci. 26, 677–693.

Percival, J.A., Sullivan, R.W., 1988. Age constraints on the evolution of the Quetico Belt, Superior Province. Canada. Geol. Surv. Can., Paper 88-2, pp. 97–108.

Pettigrew, N.T., Hattori, K.H., Percival, J.A., 2001. The Quetico intrusions, Archean examples of Alaskan/Ural type intrusions. Abstract of the Western Superior Transect Lithoprobe Meeting.

Pettigrew, N.T., Hattori, K.H., 2002. Palladium–copper-rich platinum-group element mineralization in Legris Lake mafic–ultramafic complex, Western Superior Province, Canada. Trans. Inst. Min. Metall. 111, B-46–B-57.

Pigage, L.C., Greenwood, H.J., 1982. Internally consistent estimates of pressure and temperature: the staurolite problem. Am. J. Sci. 282, 943–969.

Pirie, J., Mackasey, W.O., 1978. Preliminary examination of regional metamorphism in parts of Quetico metasedimentary belt, Superior Province, Ontario. In: Fraser, J.A., Heywood, W.W. (Eds.), Metamorphism in the Canadian Shield. Geol. Surv. Can., Ottawa, Canada, Paper 78–10, pp. 37–48.

Platt, J.P., 1986. Dynamics of orogenic wedges and the uplift of high-pressure metamorphic rocks. Geol. Soc Am. Bull. 97, 1037–1053.

Plyusnina, L.P., 1982. Geothermometry and geobarometry of plagioclase-hornblende bearing assemblages. Contrib. Mineral. Petrol. 80, 140–146.

Polat, A., Kerrich, R., Wyman, D.A., 1998. The late Archean Schreiber-Hemlo and White River-Dayohessarah greestone belts, Superior Province: collages of oceanic plateaus, oceanic arcs, and subduction–accretion complexes. Tectonophysics 289, 295–326.

Polat, A., Kerrich, R., 1999. Formation of an Archean tectonic mélange in the Schreiber-Hemlo greenstone belt, Superior Province, Canada: Implications for Archean subduction–accretion process. Tectonics 18 (5), 733–755.

Powell, R., Holland, T., Worley, B., 1998. Calculating phase diagrams involving solid solutions via non-linear equations with examples using THERMOCALC. J. Metamorph. Geol. 16, 577–588.

Pye, E.G., 1964. Map 2056 (scale of 1:63360), Georgia Lake area, Thunder Bay District. Ontario Department of Mines, Toronto.

Raase, P., 1974. Al and Ti contents of hornblende, indicators of pressure and temperature of regional metamorphism. Contrib. Mineral. Petrol. 45, 231–236.

Richardson, S.W., Gilbert, M.C., Bell, P.M., 1969. Experimental determination of kyanite–andalusite and andalusite–sillimanite equilibria: the aluminum silicate triple point. Am. J. Sci. 267, 259–272.

Rollinson, H.R., 1993. Using Geochemical Data; Evaluation, Presentation, Interpretation. Longman Scientific and Technical, Harlow, UK (GBR), 352 pp.

Sakaguchi, A., 1999. Thermal maturity in the Shimanto accretionary prism, southwest Japan, with the thermal change of the subducting slab: fluid inclusion and vitrinite reflectance study. Earth Planet. Sci. Lett. 173, 61–74.

Sawyer, E.W., 1983. The structural history of a part of the Archean Quetico metasedimentary belt, Superior Province: Canada. Precambrian Res. 22, 271–294.

Schwartz, S., Lardeaux, J.M., Guillot, S., Tricart, P., 2000. The diversity of eclogitic metamorphism in the Monviso ophiolitic complex, western Alps, Italy. Geodin. Acta 13, 169–188.

Spear, F.S., 1981. An experimental study of hornblende stability and compositional variability in amphibolite. Am. J. Sci. 281, 697–734.

Spear, F.S., 1993. Metamorphic Phase Equilibria and Pressure–Temperature–Time Paths. Mineral. Soc. Am. Monogr., New York, 799 pp.

Spear, F.S., Cheney, J.T., 1989. A petrogenetic grid for pelitic schists in the system SiO_2–Al_2O_3–FeO–MgO–K_2O–H_2O. Contrib. Mineral. Petrol. 101, 149–164.

Stern, R.A., Hanson, G.N., 1991. Archean high Mg granodiorite; a derivation of light rare earth element-enriched monzodiorite or mantle origin. J. Petrol. 32, 201–238.

Stevenson, R., Henry, P., Gariepy, C., 1999. Assimilation-fractional crystallization origin of Archean sanukitoid suites; Western Superior Province, Canada. Precambrian Res. 96, 83–99.

Sutcliffe, R.H., Sweeny, J.M., Edgar, A.D., 1989. The Lac des Iles complex, Ontario: petrology and platinum-group elements mineralization in an Archean mafic intrusion. Can. J. Earth Sci. 26, 1408–1427.

Tabor, J.R., Hudleston, P.J., Magloughlin, J., 1989. Metamorphism of the Quetico Supracrustals North of the Vermillon Granitic Complex, Northern Minnesota, vol. 14. Geol. Assoc. Can., Mineral. Assoc. Can., Can. Geophys. Union Joint Annual Meeting. p. 38 (abstract).

Taira, A., 1981. The Shimanto Belt of southwest Japan and arc trench sedimentary tectonics. Recent Prog. Nat. Sci. Jpn. 6, 147–162.

Taira, A., Katto, J., Tashiro, M., Okamura, M., Kodama, K., 1988. The Shimanto Belt in Shikoku, Japan—evolution of Cretaceous to Miocene accretionary prism. Mod. Geol. 12, 5–46.

Taira, A., Pickering, K.T., Windley, B.F., Soh, W., 1992. Accretion of Japanese Island arcs and implications for the origin of Archean greenstone belts. Tectonics 11, 1224–1244.

Taira, A., Kiyokawa, S., Aoike, K., Saito, S., 1997. Accretion tectonics of the Japanes islands and evolution of continental crust. C.R. Acad. Sci. IIA 325 (7), 467–478.

Thurston, P.C., Chivers, K.M., 1990. Secular variation in greenstone sequence development emphasizing Superior Province, Canada. Precambrian Res. 46, 21–58.

Tomlinson, K.Y., Hall, R.P., Hughes, D.J., Thurston, P.C., 1996. Geochemistry and assemblage accretion of metavolcanic rocks in the Beardmore–Geraldton greenstone belt, Superior Province. Can. J. Earth Sci. 33, 1520–1533.

Williams, H.R., 1988. Geological studies in the Wawa, Quetico, and Wabigoon Subprovinces, with emphasis on structure and tectonic development. In: Summary of Field Work and Other Activities 1988. Ont. Geol. Surv., Miscellaneous Paper 141, Toronto, pp. 169–172.

Williams, H.R., 1989. Subprovince accretion tectonics in the south-central Superior Province. Can. J. Earth Sci. 27, 570–581.

Williams, H.R., 1990. Subprovince accretion tectonics in the south-central Superior Province. Can. J. Earth Sci. 27, 571–581.

Williams, H.R., 1991. Quetico Subprovince. In: Thurston, P.C., Williams, H.R., Sutcliffe, R.H., Stott, G.M. (Eds.), Geology of Ontario. Ontario Geological Survey Special vol. 4. Ont. Geol. Surv., Ontario, Canada, pp. 383–403.

Williams, M.L., Grambling, J.A., 1990. Manganese, ferric iron, and the equilibrium between garnet and biotite. Am. Mineral. 75, 886–908.

Yamamoto, K., Masutani, Y., Nakamura, N., Ishii, T., 1992. REE characteristics of mafic rocks from a fore-arc seamount in the Izu-Ogasawara region, Western Pacific. Geochem. J. 26, 411–423.

Zaleski, E., Van-Kreemen, O., Peterson, V.L., 1999. Geological evolution of the Manitouwadge greenstone belt and Wawa–Quetico subprovince boundary, superior province, Ontario, constrained by U–Pb zircon dates of supracrustal and plutonic rocks. Can. J. Earth Sci. (Revue Canadienne des Sciences de la Terre) 36 (6), 945–966.